THESIS FOR THE DEGREE OF LICENTIATE OF ENGINEERING

Integrating hydrogels and machine learning to understand digestion

Giovanni Tizzanini

Department of Chemistry and Chemical Engineering
CHALMERS UNIVERSITY OF TECHNOLOGY

Göteborg, Sweden 2025

Integrating hydrogels and machine learning to understand digestion
GIOVANNI TIZZANINI

Licentiatuppsatser vid institutionen för kemi och kemiteknik
Chalmers tekniska högskola
Nr 2025:07

Department of Chemistry and Chemical Engineering
Chalmers University of Technology
SE-412 96 Göteborg
Sweden
Telephone: +46 (0)31-772 1000

Cover:
Illustration depicting the gastrointestinal tract with a camera probe (top left), a schematic of a convolutional neural network (top right), the structure of a pectin gel (bottom left), and short-chain fatty acids (bottom right). The image was developed with assistance from ChatGPT, includes hand-drawn components, and was finalized using Affinity Designer 2.

Printed by Chalmers Dygitaltryck
Göteborg, Sweden 2025

Integrating hydrogels and machine learning to understand digestion
Thesis for the degree of Licentiate of Engineering
GIOVANNI TIZZANINI

Department of Chemistry and Chemical Engineering
Chalmers University of Technology

Abstract

Understanding the behavior of food materials during digestion is essential for advancing nutritional strategies that support individuals' health. In this study, I aim to investigate the digestive behavior of gelatin and pectin/polygalacturonic acid (PGA) gels, as model biopolymers, across different regions of the gastrointestinal tract. I also explore whether computer-assisted analysis of videos recorded during the digestion of gelatin gels can be used to determine digestion and physiological conditions.

I focused on the gastric digestion of gelatin gels crosslinked with transglutaminase (TGase), showing their stability under gastric conditions and demonstrated that convolutional neural networks (CNNs) combined with multilayer perceptrons (MLPs) have the potential to predict the degree of hydrolysis (DH) and classify digestive environments from visual features alone. To elaborate further, I examined how chemical modifications, e.g., methylation and hydrolysis, influenced the structure and rheological properties of pectin and PGA. These changes affected gel network parameters such as mesh size, turbidity, and viscosity, which are potentially linked to digestion behavior. The fermentability of modified pectin using *in vitro* human colonic fermentation showed that pectin of low molar mass and pectin fed as gel produced higher total short-chain fatty acids (SCFAs) than higher molar mass or dispersed forms, highlighting the importance of matrix structure in modulating microbial activity. These findings enhance our understanding of the digestion of food materials, and show potential for the use of neural networks in probing digestion from images.

Keywords: Pectin, gelatin, polygalacturonic acid, *in vitro* digestion, *in vitro* fermentation, gel, mesh size

List of Publications

This thesis is based on the following appended manuscripts:

Manuscript I:
Predicting *in vitro* digestion of gelatin gels using machine and representation learning for image processing
Giovanni Tizzanini, Jakob Ytterberg, Martin Längkvist, Patricia Lopez-Sanchez, and Anna Ström
Manuscript

Manuscript II:
Impact of Methyl-esterification on the Microstructure of Calcium-Induced Polygalacturonic Acid Gels
Mikaela Börjesson, Giovanni Tizzanini, Anna Ström, Adrien Lerbret, Fabrice Cousin, Ali Assifaoui
Manuscript under revision

My Contribution

Manuscript I:
I planned and performed the video recordings and the experiments of compression tests, rheology, swelling, and degree of hydrolysis. I interpreted the results and wrote the first draft of the manuscript, which is being finalized together with my co-authors.

Manuscript II:
I carried out the molecular mass analysis through size exclusion chromatography (SEC-MALS), and elaborated the data. I integrated the results in the manuscript. Further, I had specific responsibility of integrating current knowledge of calcium pectin gelation with findings from neutron scattering and molecular dynamics.

"What he told you that day was the secret of life itself.
One lives and survives only if one has the ability
to swallow and digest bitter and unpalatable things.
We, you and I, and our people shall live because there
are only a few among us who do not love raw onions."

— *Jamil Ahmad, The Wandering Falcon*

Notation

AA	Amino acid
AAA	Aromatic amino acid
AI	Artificial intelligence
ATR-FTIR	Attenuated total reflectance - Fourier transform infrared spectroscopy
CNN	Convolutional neural network
DF	Dietary Fiber
DM	Degree of methylation
DTT	DL-dithiothreitole
GalA	Galacturonic acid
GDL	Glucono-δ-lactone
GIT	Gastrointestinal tract
HG	Homogalacturonan
HMP	High methoxyl pectin
HPLC	High-performance (or pressure) liquid chromatography
HSV	Hue, saturation, and value
LMP	Low methoxyl pectin
ML	Machine learning
MLP	Multi-layered-perceptron
OPA	O-phthaldialdehyde
PGA	Polygalacturonic acid
Phe	Phenylalanine
RG	Rhamnogalacturonan
RMSE	Root mean square error
SANS	Small-angle neutron scattering
SCFA	Short-chain fatty acid
SEC-MALS	Size exclusion chromatography-multiangle light scattering
TGase	Transglutaminase
Trp	Tryptophan
Tyr	Tyrosine
VOC	Volatile organic compound
XGA	Xylogalacturonan
WCE	Wireless Capsule Endoscopy

Contents

1 Introduction

The gastrointestinal tract (GIT) carries out the function of nutrient absorption, and it plays a central role in the host physiology, including their health [1, 2]. Understanding how food materials behave during digestion is key for developing nutritional strategies that support health and individuals' dietary needs, particularly for vulnerable populations, such as the elderly or subjects affected by gastrointestinal conditions [3–6]. However, current *in vivo* and *in vitro* models face limitations in realism, accessibility, or cost [7, 8].

Gelatin, a denatured form of collagen, forms thermo-reversible proteic gels via physical crosslinks and can be further connected by enzymatic crosslinking using transglutaminase (TGase) [9]. Pectin, a plant-derived polysaccharide and dietary fiber (DF), is composed primarily of homogalacturonan (HG), a linear polymer of 1,4-α-D-galacturonic acid residues [10]. Chemical or enzymatic de-esterification of HG yields polygalacturonic acid (PGA), which, like pectin, forms ionotropic gels in the presence of divalent cations such as calcium through the egg-box model [11].

In this thesis, I explored how the physicochemical properties of biopolymers influence their digestion and investigated the potential of applying and integrating machine learning (ML) tools to predict digestive conditions using imaging and video data. The primary objective was to investigate whether visual changes in biopolymer gels can be correlated with digestive conditions. To achieve this, I aimed at developing an *in vitro* system to record the degradation of gelatin gels on video, enabling the collection of relevant data for ML analysis. I studied in detail gelatins behavior under digestive conditions, serving as a foundational model, and in parallel, I also explored pectin and its simpler form, PGA, hydrogels in order to later apply the same ML techniques to those systems. Another key aspect of my work involved examining how the physical form of pectin affects its fermentability *in vitro*. These efforts were guided by the hypothesis that visual changes in gelatin gels can be related to digestive conditions, and can be extrapolated to other macronutrients digestion.

2 Background

Understanding how food behaves in the GIT is important for advancing research in food science and human health. Digestion, extending from the oral cavity to the large intestine, is central not only for nutrient absorption but also for regulating metabolic, immune, and neurological responses.

Polymer-based hydrogels such as pectin and gelatin are of particular interest due to their dual role as dietary components and model systems [12].

This section outlines the digestive system in the context of experimental food science, with a focus on gelatin and pectin hydrogels and their structural response to digestion. It concludes with an outlook on applying machine learning (ML) to analyze *in vitro* data and support the development of more predictive digestion models.

2.1 Gastrointestinal tract and digestion

The human GIT comprises several organs, among which the mouth, stomach, small intestine, and large intestine are the most relevant; each of these performs specialized roles in the digestion and absorption of nutrients. Salivary amylases are responsible for the first carbohydrate breakdown in the mouth [13], while the acidic environment of the stomach facilitates protein hydrolysis by pepsin [14]. In the small intestine, a mix of enzymes from the pancreas and bile from the liver further break down various compounds: lipids are emulsified by bile salts and cleaved by lipases into fatty acids and monoglycerides; proteins are further cleaved by proteases like trypsin and chymotrypsin, while carbohydrates are hydrolyzed by enzymes like amylases and disaccharidases [15]. The epithelial lining of the small intestine maximizes nutrient absorption, while the large intestine focuses on water resorption and houses a diverse microbiota responsible for fermenting DF and producing short-chain fatty acids (SCFA) [13]. On top of the chemical action, mechanical actions like chewing, mixing, and peristalsis aid digestion by increasing surface area and ensuring enzyme contact and food movement along the tract.

Understanding the mechanical and biochemical environment of the GIT is key to evaluating how DF, proteins, and other macronutrients behave in our body. This is especially critical for the more fragile demographic groups, as the aging population and those with digestive disorders, where changes in physiology can

significantly alter nutrient absorption, metabolic outcomes, and therefore, health [4, 16]. To mimic these complex environments, researchers use *in vitro* systems replicating pH, ionic environment, and enzymatic activity typical of each GIT compartment [17]. Advanced models can simulate peristalsis and fluid dynamics using artificial membranes and flow control systems[8].

2.1.1 Digestive models

The scientific investigation of digestion relies on three principal experimental approaches: *in vitro*, *in vivo*, and *ex vivo* models. Each of these methods offers advantages and limitations. *In vitro* digestion systems are laboratory-based models designed to simulate various parts of the GIT [17], and are categorized as either static or dynamic models. Static models, like the pH-stat method [18] and the INFOGEST protocol [19], are used for their simplicity, reproducibility, and cost-efficiency. However, they do not capture physiological dynamics such as peristalsis or gradual enzymatic release and nutrient adsorption. In contrast, dynamic systems, such as the SIGMI® model [20], SHIME® model [21], and TIM models [8, 17], rely on computer-controlled environments to mimic real-time changes in pH, enzyme concentrations, and transit times, providing a more realistic but costlier alternative.

In vivo methods involve studies conducted on living organisms, typically humans [22] or animal models [23–25]. These techniques include breath tests, biopsy samples, and more advanced imaging technologies. While physiologically relevant, they are expensive, time-consuming, and ethically constrained. *ex vivo* approaches, such as colonic fermentation using human fecal samples [26] or tissue cultures [27], provide a bridge between *in vitro* and *in vivo* techniques. These approaches maintain biological functionality while enabling a more controlled environment than *in vivo* studies [28].

Despite all these models, accurately replicating digestive processes remains a challenge, and requires integrating dynamicity and host complexity [7], potentially through the integration of machine learning to enhance predictive power and interpretability.

2.2 Hydrogels

Gelatin and pectin are part of the human diet and are used as biopolymers in the food and pharmaceutical industries, owing to their foaming, emulsifying, gelling, and film-forming properties, particularly used in encapsulation technologies, drug delivery systems, and food texturizers [29–31]. Knowing where and how these polymers break down in the body helps improve their use in food and pharma formulations.

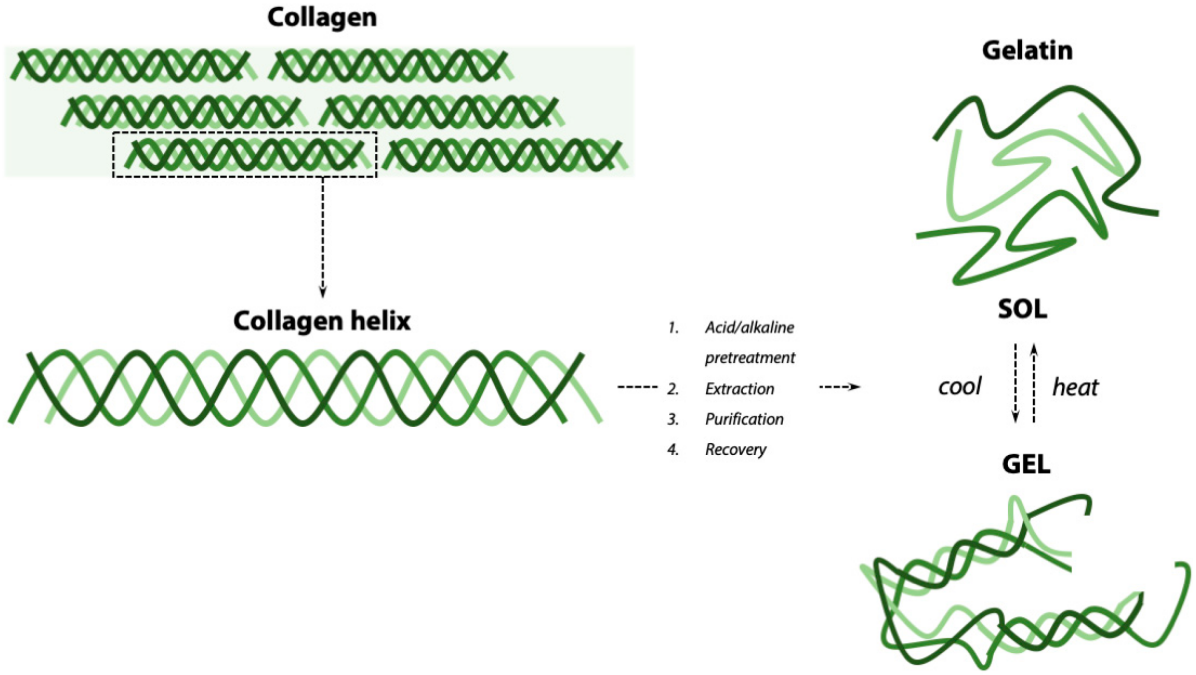

Figure 2.1: *Schematic of the gelatin extraction from collagen (left) and reversible gelatin gel formation (right). Reproduced with permission from Campiglio et al., Materials 2019 [38].*

2.2.1 Gelatin

Gelatin is a polymeric substance and a multi-functional ingredient obtained by the partial hydrolysis and heat denaturation of skin, bones, and connective tissue collagen (see Figure 2.1) [32]. Source and extraction conditions determine most of the physicochemical properties of the gelatin, such as type and bloom strength, which directly influence gelatin gels' T_{m}, viscosity, and mechanical properties [29]. Type A and type B gelatin are produced through the partial hydrolysis of collagen by acid or alkali, respectively [33]. Generally, type A gelatin is obtained from pigs, poultry, and fish, whereas type B gelatin is obtained from bovine sources [34]. Deamidation of asparagine and glutamine due to alkaline conditions leads type B to have more negatively charged amino acids (AAs) [34], and thus a lower isoelectric point (pI) of 5, compared to the ∼7 of type A gelatin [35, 36].

Gelatin dissolves in hot water and forms thermoreversible gels upon cooling, typically at temperatures between 20 and 35 °C, depending on the gelatin type [37]. This sol-gel transition is driven by the conformational change of gelatin chains from random coils at high temperatures to partial triple-helix structures upon cooling, mimicking the native collagen configuration, as illustrated in Figure 2.1 [32]. These triple-helix junctions form a crosslinked network that gives rise to the gel.

The bloom strength, or bloom number, is divided into low and high, of around

30-125 g and 200-300 g, respectively [37]. The bloom strength corresponds to an average molar mass, where low bloom corresponds to lower (20-25 kDa) and high bloom to higher (50-100 kDa) molar mass [39]. The bloom strength is measured in grams using a standardized method of measurement that evaluates how many grams the gel can hold before breaking [40]. Therefore, higher molar mass means longer gelatin chains, which form more triple helices, creating a stiffer and firmer gel [39]. This more extended network also influences the melting temperature, which, depending on the bloom, lies between 23 °C and 35 °C, for low and high bloom, respectively [37]. Gelatin gels can be further crosslinked by using enzymes as TGases, which catalyze the formation of ε-(γ-glutamyl)-lysine (G-L) crosslinks by three steps, namely acyl transfer, crosslinking, and deamidation reactions [9, 29], causing the rise in T_{m} of the gel.

The swelling behavior and mechanism of gelatin hydrogels have been studied for a long time [41], and it is strongly influenced by pH, salt concentration, and crosslinking density. As a polyampholyte, it exhibits swelling behavior sensitive to ionic conditions due to ion pair formation between its charged groups and counterions [42]. Salt addition can stabilize the gel network by modulating electrostatic interactions, especially near the isoelectric point, where swelling decreases sharply [43]. Increased crosslinking density limits chain mobility and reduces swelling [39], while higher temperatures enhance it by disrupting hydrogen bonds; in contrast, higher gelatin concentrations lead to reduced swelling [43].

Gelatin undergoes enzymatic hydrolysis in the stomach and small intestine. It has been used as a model protein to study digestion and absorption dynamics in both animal [44] and human studies [45]. Its digestibility has made it particularly relevant in the pharmaceutical industry, where it is commonly used in capsules and films [37]; these forms have been shown to be enzyme-digestible and absorbed *in vivo*, with *in vitro* tests offering reasonable predictions of *in vivo* behavior [46, 47]. In the food industry, gelatin is employed for its textural and gelling abilities, for example, in replacing animal fat in food formulations [48]. Finally, its mechanical properties can be enhanced through enzymatic treatments such as TGase, which has been shown to improve fish gelatin mechanical properties [49, 50] and in developing composite probiotic delivery systems, for example, with pectin [51].

2.2.2 Pectin and polygalacturonic acid (PGA)

Pectin is a complex plant-derived polysaccharide found in plant cell walls, with apple and citrus fruits being the primary sources for commercial pectins. Conventional extraction methods typically involve heating the plant material in an acidified buffer with agitation, which promotes the hydrolysis of protopectin into soluble pectin [30]. This process may also include the use of chelating agents to enhance yield. Alternatively, pectin can be extracted under alkaline conditions,

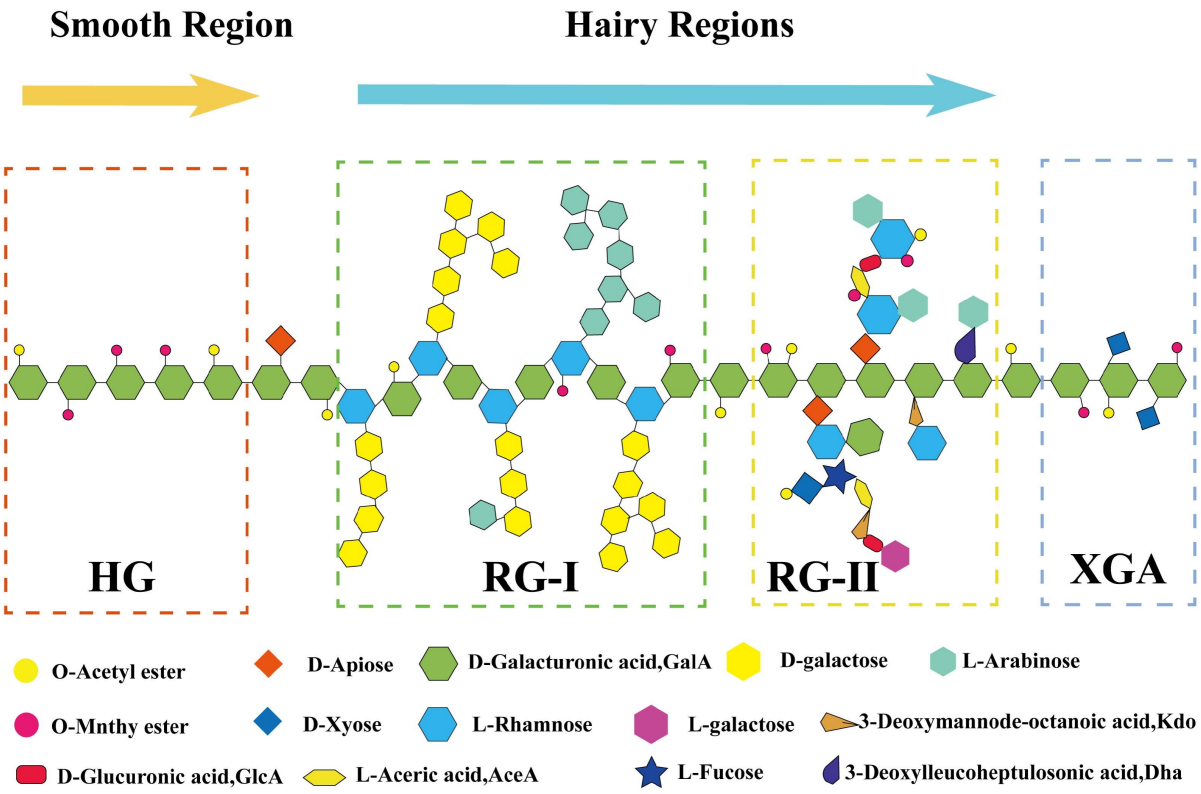

Figure 2.2: *Schematic representation of pectin structure. Pectin's regions are homogalacturonan (HG), rhamnogalacturonan I (RG-I), xylogalacturonan (XGA), and rhamnogalacturonan II (RG-II). Reproduced with permission from Yue et al., International Journal of Biological Macromolecules 2023 [53].*

though this approach generally results in significantly lower yields [30]. Pectin is primarily composed of 1,4-α-D-galacturonic acid residues arranged in linear homogalacturonan (HG) regions, which make up the majority of its backbone [10]. It also contains domains such as rhamnogalacturonan I (RG-I), xylogalacturonan (XGA), and rhamnogalacturonan II, having neutral sugars branching off the main HG backbone [10] (see Figure 2.2). De-esterification of HG converts methoxyl groups into carboxyl groups, leading to the sole polygalacturonic acid (PGA) [11]. Source and extraction method influence the pectin structure, as the relative abundance of the four different regions, and its monosaccharide composition [31, 52].

Another critical parameter for pectin is the degree of methylation (DM). DM corresponds to the percentage of carboxyl groups in the HG backbone esterified with methanol, and it is also called degree of esterification or methyl-esterification [54]. The DM splits pectin into two main subcategories, high methoxyl pectin (HMP, DM $>$ 50 %) and low methoxyl pectin (LMP, DM $<$ 50 %) [55]. HMP forms gels in the presence of sucrose ($>$ 55 %) and acid ($<$ pH 3.6) [56], since high sucrose concentration reduces water activity and promotes hydrophobic

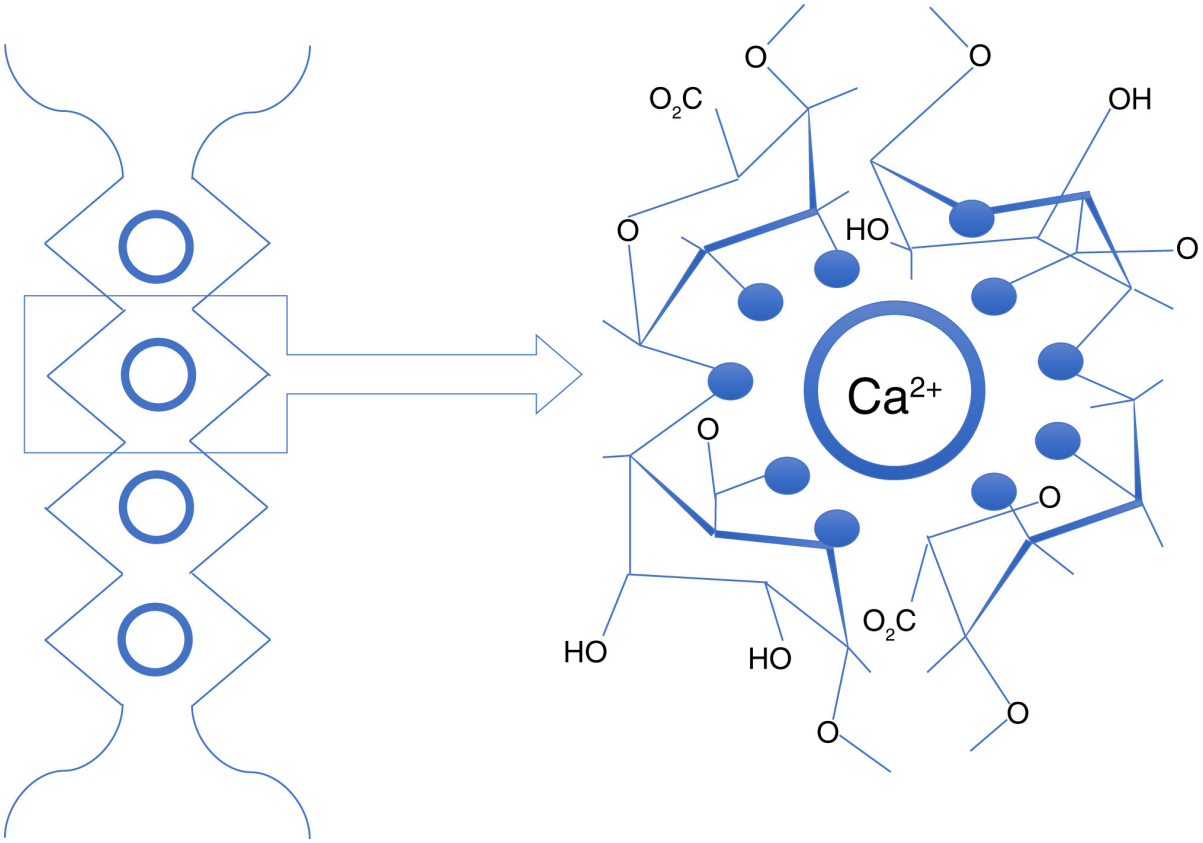

Figure 2.3: *Scheme of the egg-box structure and dimerization between Ca^{2+} (unfilled circles) and the oxygen atoms (filled circles) within HG-blocks (zigzags). Reproduced with permission from Templeman et al., Journal of the Science of Food and Agriculture 2018 [62].*

interaction of methoxyl groups, while low pH reduces carboxyl group protonation and electrostatic repulsion. Non-protonated carboxyl groups can then form hydrogen bonds with secondary alcohols [57]. Another main gel mechanism happens in the presence of divalent cations such as calcium ions, which can be expressed by the "egg-box" model. Here, the cations can crosslink the pectin molecule to form an ionotropic gel network [58], as shown in Figure 2.3. To form a stable junction connecting the pectin network, six to twenty continuous non-methoxylated GalA units are required for pectin [59, 60]. Other mechanisms have been proposed to occur alongside the egg-box model, including the formation of localized or point-like crosslinks [61].

Pectin is a common polysaccharide in the human diet, and, as a dietary fiber, resists digestion in the upper GIT and reaches the large intestine, where the gut microbiota ferments it. This fermentation process, similar to that of other dietary fibers, produces beneficial short-chain fatty acids (SCFAs) such as butyrate and propionate, which contribute to host health [63]. Consequently, pectin

has been studied in fermentation models [64, 65] to evaluate, for instance, its effects on human stool characteristics [66] or on human microbiota composition [67]. Notably, a recent study investigated the fermentation of pectin in gel form, especially focusing on particle size [68]. I expanded on this by comparing fermentation of bigger gel particles versus dispersed forms of the same LMP.

2.3 Machine learning (ML)

ML, a subfield of artificial intelligence (AI), is a powerful and versatile tool with broad scientific applications. ML focuses on algorithms that learn from data and generalize to new inputs with minimal explicit programming. One key strength of ML is its ability to analyze visual data by automatically identifying and quantifying complex or subtle patterns, often difficult to detect using conventional techniques [69, 70]. In the context of digestion research, ML has the potential to be integrated into non-invasive, real-time monitoring approaches. For instance, combining electronic nose (e-nose) sensor arrays with ML enables the detection of volatile organic compounds (VOCs) associated with digestion, offering insight into gastrointestinal processes [71]. Additionally, in medical diagnosis, CNNs have been used to classify gastrointestinal pathologies from wireless capsule endoscopy (WCE) images [72], while more recently, vision transformer models have demonstrated improved accuracy in diagnosing gastrointestinal disorders from endoscopic images [73].

3 Methodology

3.1 Sample preparation

3.1.1 Materials

Gelatin type A (Bloom 300 g, porcine skin), pepsin A from porcine gastric mucosa (lyophilized powder, ≥2,500 U/mg), sodium tetraborate decahydrate, DL-dithiothreitole (DTT), and sodium dodecyl sulfate (SDS) were purchased from Sigma-Aldrich, USA. Hydrochloric acid (2 M) and calcium chloride dihydrate were acquired from Sigma-Aldrich, Germany. Phthaldialdehyde 97 % (OPA) was purchased from Sigma-Aldrich, China, and sodium chloride from Acros-Organics, Spain. Transglutaminase (TGase, Galaya®Prime) was bought by Novozymes, Denmark, while the yellow food coloring dye (Dr. Oetker) was shopped in Sweden. Low Methoxyl pectin (LMP) was purchased from Herbstreith & Fox, Germany. Calcium carbonate and glucono-δ-lactone (GDL) were purchased from Fisher-Scientific, UK. Polygalacturonic acid (PGA), sodium chloride, calcium chloride dihydrate, NaOH, and $NaNO_3$ were purchased from Sigma-Aldrich, USA. Analytical grade absolute methanol and ethanol was purchased from VWR, France.

3.1.2 Alkaline hydrolysis of pectin

The alkaline hydrolysis of pectin was based on the method described by Hunter *et al.* [74]. The initial pectin concentration was set to 1.0 %, temperature to 25 °C, and pH to 10.0. For this, a 2.0 g portion of pectin was added to 200 ml of a solution of sodium hydroxide in a distillation flask, and the mixture was refluxed for 24 hours. At the end of each test, the hydrolyzate was cooled in an ice bath and immediately neutralized with HCl 2 M.

3.1.3 Methylation of polygalacturonic acid

As described by Rosenbohm *et al.* [75], methylation of PGA was performed by slowly adding 200 mL of cold methanol to 10 mL of acetyl chloride and stirring for 1 hour. Then, 3 g of PGA was added, and the mixture was stirred in a sealed flask at 8 °C for 1, 5, or 10 days. After each period, the partially methylated PGA (MeO-PGA) was filtered, washed with 60 % HCl-acidified aqueous ethanol

followed by absolute ethanol, and dried under vacuum at room temperature. The degree of methylation (DM) was determined by FTIR.

3.1.4 Preparation of gels

TGase-crosslinked gelatin gels: The method to cast the gels was adapted from Mao *et al.* [76]. Gelatin powder (3%) was swollen in Milli-Q water at room temperature for 30 minutes under continuous stirring. The temperature was then raised to 45 °C, and yellow food dye (10 $\mu L/mL_{gel}$) was added, followed by TGase (433 $U/g_{gelatin}$, equivalent to 13 U/mL_{gel}). The mixture was stirred continuously for 25 min before TGase was deactivated by heating in an 80 °C water bath for 5 min. The gel was poured into molds and allowed to cool at room temperature. The yellow dye was included to monitor color changes in video recordings, indicating swelling and material loss. The gels were cast into various molds and left to set overnight before use. The molds were a Plexiglas cylindrical mold with dimensions of 9.5 mm h, 12 mm ⌀, and the camera probe (IP67, Staright) hollow tip, of dimensions of 2 mm h and 7 mm ⌀(Figure 3.1b). Both molds were sealed to prevent evaporation.

Calcium-induced pectin gels: Pectin gels were prepared using a method originally proposed for alginate by Draget *et al.* [77]. GDL and $CaCO_3$ were freshly dispersed in water and then mixed with a pectin solution. Calcium release from the carbonate salt was triggered by the gradual acidification resulting from the hydrolysis of GDL, which naturally occurs in water, and allowed for a gradual release of Ca^{2+} ions and a homogeneous gel. A 2:1 molar ratio of calcium to GDL was employed, and the final calcium concentration after release was 52.5 mmol/L. A 3% pectin gel was prepared for *in vitro* fermentation experiments. All procedures were performed in a glovebox to ensure gel sterility and anaerobic environment.

Calcium-induced PGA and methylated PGA gels: PGA or MeO-PGA powders were dispersed in 10 mM NaCl and stirred for 2 h. The pH was adjusted to 5.5 (2 units above the pK_a of PGA) using NaOH to ensure solubilization and conversion to sodium galacturonate. Solutions were dialyzed three times for 2 h against 10 mM NaCl using dialysis membranes with a 3.5 kDa molar mass cutoff. A 100 mM $CaCl_2{\cdot}2H_2O$ solution in 10 mM NaCl was prepared for gelation. Hydrogels were prepared following the protocol described by Maire du Poset *et al.* [78] (see Figure 3.1a). 5 mL of the 20 g/L polymer solution was poured into a glass tube (2.1 cm diameter) sealed at the bottom with a dialysis membrane. The tube was immersed in 50 mL of the calcium solution for 24 hours. The setup was covered with paraffin film to minimize evaporation. Gels were sliced at different distances z from the membrane, and thicknesses were measured after cutting. Slice 1 corresponds to the region nearest the membrane, while Slice 4 is the farthest.

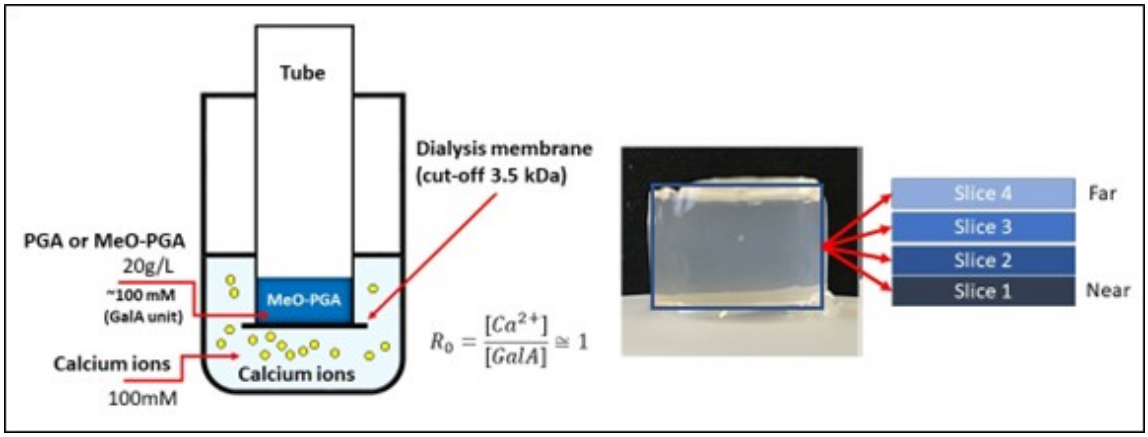

(a)

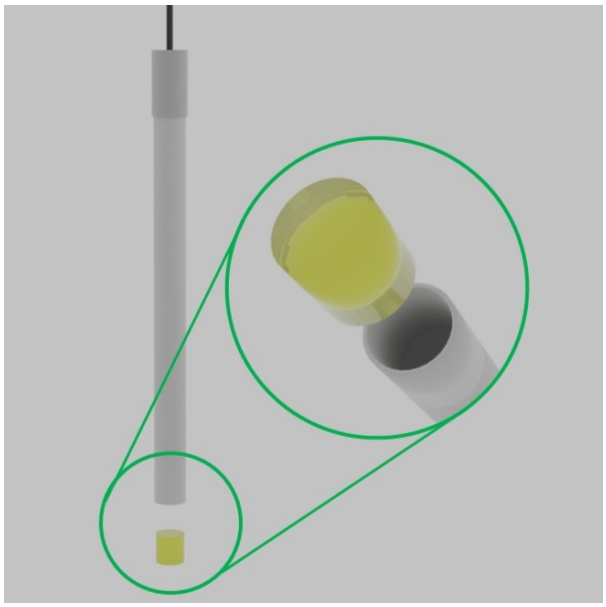

(b)

Figure 3.1: *Images of the calcium-induced PGA gels used in Manuscript II (a) and the microscope probe and its tip that was coated with custom casting of the TGase-crosslinked gelatin used for video collection in manuscript I (b).*

3.2 Chemical and mechanical characterization of the gels

3.2.1 Fourier transform infrared (FTIR) spectroscopy

The DM of pectin, hydrolyzed pectin, and MeO-PGA was determined using Fourier-transform infrared (FTIR) spectroscopy. Measurements were performed with a Perkin-Elmer Spectrum 65 spectrometer (Perkin-Elmer, France), equipped with an attenuated total reflectance (ATR) accessory (Miracle Pike) using a Ge crystal. Each spectrum was collected over the 600-4000 cm^{-1} range with 16 scans

and a resolution of 2 cm^{-1}. DM, defined as the ratio of esterified to total carboxylic groups, was calculated from the peak areas at 1736 cm^{-1} (ester C=O stretch) and 1630 cm^{-1} (carboxylate COO^- stretch), following the method described by [79]. Peak deconvolution was performed using OriginPro (OriginLab Corporation, Northampton, MA, USA). Both -COOH and -COOMe groups contribute to the 1736 cm^{-1} signal ([80]). Since unmodified PGA contains only -COOH groups (i.e., DM = 0 %), its contribution at 1736 cm^{-1} was subtracted from that of the rest of the samples, and DM was computed using the following equation:

$$DM(\%) = \left(\frac{A_{1736}}{A_{1736} + A_{1630}}\right) - \left(\frac{A_{1736,\mathrm{PGA}}}{A_{1736,\mathrm{PGA}} + A_{1630,\mathrm{PGA}}}\right) \tag{3.1}$$

3.2.2 Molar mass determination by size exclusion chromatography

The number- and weight-averaged molar masses (M_n and M_w) of PGA and MeO-PGA were determined using size exclusion chromatography with multi-angle light scattering (SEC-MALS). Due to PGA's tendency to aggregate in solution [81], the following sample preparation was employed. Powders were pre-wetted with ethanol for 30 min, then dispersed in Milli-Q water for 4 h with 0.02 % w/w NaN_3 to prevent microbial growth. Samples (2 mg/mL) were adjusted to pH 7 using 0.1 M NaOH, allowed to swell overnight at room temperature, then heated at 90 °C for 30 min and sonicated for another 30 min. Solutions were passed through an ion-exchange column (EconoFit Macro-Prep High S, 7 × 25 mm, 0.3 mL/min), centrifuged (17,000 g, 15 min), and diluted to 1 mg/mL, matching the concentration of the eluent (20 mM $NaNO_3$ containing 0.002 % w/w NaN_3).

The mobile phase was filtered (0.22 µm MCE membrane, MF-Millipore, Merck) and degassed via sonication. Before injection, samples were filtered (Acrodisc 13 mm syringe filter, 0.45 µm PTFE). A Tosho TSKgel GMPWXL column (7.8 × 300 mm, 13 µm) with a Tosho guard column (PWXL, 6.0 × 40 mm, 12 µm) and an inline filter (0.05 µm, Millipore VM) were used. The injection volume was 100 µL, and the flow rate was 0.5 mL/min. The HPLC system (Agilent 1260 Infinity II) included a degasser, quaternary pump, and autosampler. Detection was performed using a DAWN HELEOS-II multi-angle light scattering detector, a Viscostar 3 viscometer, and an Optilab rEX refractive index detector. Data were analyzed with ASTRA software (v7.3.2). Each sample was analyzed in triplicate.

3.2.3 Rheology

Rotational rheology: Viscosity was measured using an Anton Paar MCR 302 rheometer equipped with a sandblasted plate-plate geometry (50 mm diameter, 1 mm gap). Measurements were conducted at 22 °C, maintained by a

VISCOTHERM VT2 water bath. A shear rate sweep from 1 to 50 s^{-1} was performed. To determine the overlap concentration (C^*), PGA solutions with varying DM and concentrations (5-20 g/L) were analyzed. For C^* comparison, viscosity was recorded at 20 s^{-1}. The viscosity of 3 pectin solution at pH 6 was determined using a DHR-3 rheometer (TA Instruments, New Castle, USA), and the same geometry was used, but with a static shear stress of 50 s^{-1}. Three replicates per sample were measured.

Oscillatory rheology: Storage (G') and loss (G'') moduli were determined using a DHR-3 rheometer (TA Instruments, New Castle, USA) with a 40 mm diameter parallel plate geometry and a 400 µm gap. Temperature was controlled with a Peltier plate, and evaporation was prevented using a solvent trap and a TA Instrument custom-built cover. Oscillatory measurements were performed in triplicate on a 3% gelatin solution in MQ water, with or without TGase. The sample was heated to 45 °C, held for 25 min, then ramped to 80 °C at 5 °C/min, held for 5 min, cooled to 25 °C at 5 °C/min, and set for 1 h. The temperature was increased to 37 °C at 1 °C/min and held for 1 h, followed by a rise to 60 °C for 1 h for TGase-containing samples. Strain and frequency were fixed at 1 % and 1 Hz.

3.2.4 Gel compression tests

Uniaxial compression tests were conducted on the unswollen gelatin gels, both with and without TGase crosslinking, using an Instron 68TM-5 testing machine (USA) equipped with a 5 kN load cell. Experiments were carried out at room temperature, with data acquisition managed through Bluehill 2 software. Each gel sample was carefully positioned and centered between stainless steel compression plates. The compression was applied at a constant deformation rate of 0.2 mm/s, and seven replicates were tested per sample type. Both compressive stress and strain were recorded throughout the measurements.

3.3 Swelling and digestion of gels

3.3.1 Media compositions

The swelling and the digestion of the gelatin gel were studied in media with different compositions, whose acronyms are given in Table 3.1. The values of pH were adjusted using HCl 2 M, and the ionic strength was adjusted by dissolving NaCl and $CaCl_2$ salts.

Gelatin gel cylinders (9.5 mm height, 12 mm diameter) were immersed in 20 mL of various media at 37 °C for 0, 15, 30, 60, and 180 minutes. After the specified time, the swollen cylinders were weighed after gently dabbing to remove excess water.

Table 3.1: *Media composition for swelling tests, degree of hydrolysis through the o-phthalaldehyde method, video recordings and analysis. "I" stands for ionic strength corresponding to "intestinal" (142 mM), while "S" stands for ionic strength corresponding to "gastric" (98 mM) compartments. The ionic strength was achieved through dissolution of NaCl (and 0.15 mM of $CaCl_2$ for media containing pepsin). pa, pb, and pc stand for a pepsin concentration of 150, 310, and 750 U/ml, respectively.*

Medium	**pH**	**ionic strength (mM)**	**Pepsin concentration (U/mL)**
70	7.0	0	–
7S	7.0	98	–
7I	7.0	142	–
30	3.0	0	–
3S	3.0	98	–
3I	3.0	142	–
3Spa	3.0	98	150
3Spb	3.0	98	310
3Spc	3.0	98	750
2S	2.0	98	–
2Spa	2.0	98	150
2Spb	2.0	98	310
2Spc	2.0	98	750
1.5S	1.5	98	–
1.5Spa	1.5	98	150
1.5Spb	1.5	98	310
1.5Spc	1.5	98	750

The swollen weight (W_s) was recorded, followed by drying at 80 °C overnight to obtain the dry weight (W_d). Each sample was replicated 3 times. Water uptake (Q_{s}) was calculated using [82]:

$$Q_{\mathrm{s}} = \frac{W_{\mathrm{s}} - W_{\mathrm{d}}}{W_{\mathrm{d}}} - Q_{\mathrm{s0}} \tag{3.2}$$

To fit the swelling data, the empirical Fick diffusion model was applied [83]:

$$F = kt^n \tag{3.3}$$

where F is the fractional uptake at time t, k is a constant, and n is the diffusion exponent indicating the transport mechanism.

3.3.2 Degree of hydrolysis determination by O-phthalaldehyde method

DH was determined using the OPA method in triplicate [84]. OPA reagent was prepared by dissolving 3.8 g sodium tetraborate decahydrate and 0.1 g sodium dodecyl sulfate in 75 mL Milli-Q water, then adding 80 mg OPA and 88 mg DTT, followed by dilution to 100 mL with water. Serine was used as a standard in the 0.185-0.95 mmol/L range, with five repetitions per concentration. Blank and negative samples (gelatin without digestive enzyme) were also measured. Samples were centrifuged at 4 °C (10 min, 10,000×g) before adding 30 µL of the sample and 230 µL of reagent to a 96-well plate. After 120 seconds at room temperature, absorbance was measured at 340 nm. The DH was calculated as:

$$DH\ (\%) = \frac{Total\ NH_2\ (\text{tabulated})}{NH_2\ (\text{sample})} \times 100 \tag{3.4}$$

where NH_2(sample) is the concentration of free amino groups in the sample after blank correction, and total NH_2(tabulated) is the total free amino groups from acid hydrolysis of gelatin, as referenced. The Michaelis-Menten equation for enzyme kinetics was used to fit the DH results and interpolate its values:

$$\frac{dDH}{dt} = \frac{V_{\max} \cdot [S]}{K_{\mathrm{m}} + [S]} \tag{3.5}$$

Where $\frac{dDH}{dt}$ is the rate of the hydrolysis, V_{max} is the maximum rate of the reaction, $[S]$ is the substrate concentration, and K_m is the Michaelis constant. The DH at disappearance for each video was obtained by interpolating the DH at the observed disappearance time.

3.4 Video recording and analysis

3.4.1 Video recording

The camera microscope (Figure 3.1b), with gel at its tip, was immersed in 20 mL of media with different compositions (Table 3.1). All recordings were conducted at 37 °C in the neutral booth setup (Figure 3.2). A white sheet provided a constant background, and ambient lighting (Streamplify Light 10 ring light) was used to normalize the illumination. The camera was positioned at a 90 ° angle to the beaker. Videos were recorded using OBS (Open Broadcaster Software) for several hours with consistent settings.

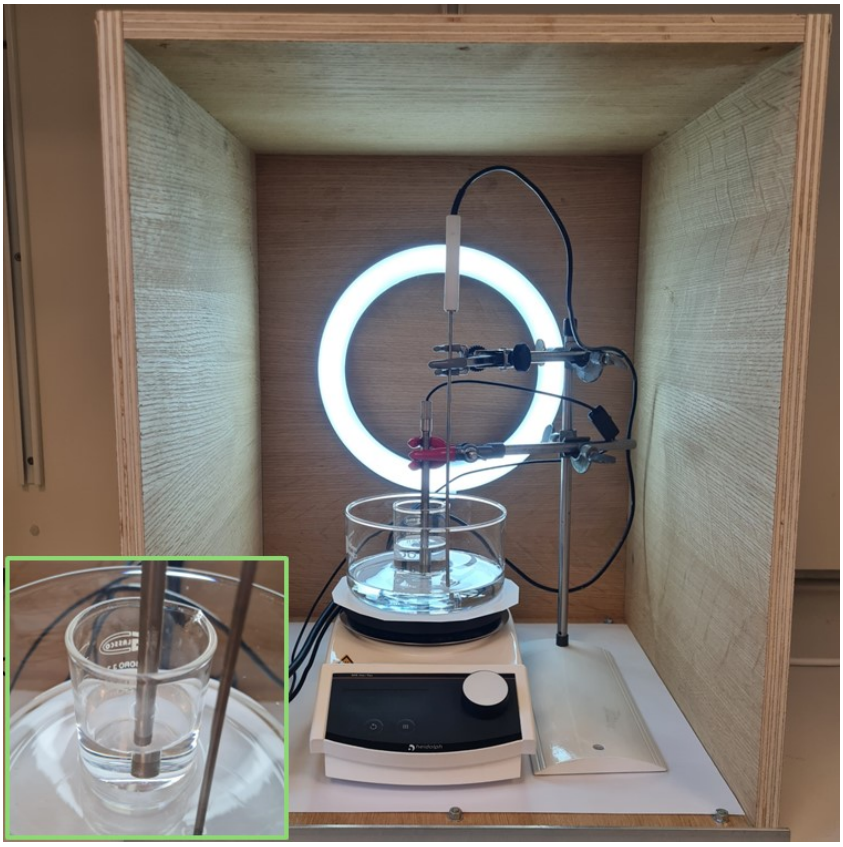

Figure 3.2: *Open neutral booth for video recordings; a close-up of the probe immersed in the beaker is shown bottom-left.*

3.4.2 Machine learning models

Video recordings of gelatin gels immersed in different media (Table 3.1) were used to train and validate the ML models in collaboration with Dr. Längkvist at Örebro University. Frames also varied in hue, saturation, and color, motivating the need for color normalization. To focus on degradation rate, models were

trained on paired frames separated by a time distance of Δt to capture structural and visual differences over time. Two models were employed: an HSV+MLP model, which takes as input the difference in hue, saturation, and value (HSV) channels between two frames at Δt (Figure 3.3a); and a CNN+MLP model, which replaces HSV processing with a convolutional neural network that learns frame representations (Figure 3.3b). The output representations from either HSV or CNN were passed to the same MLP structure for final classification. RGB conversion was initially applied, but the results were inconclusive and therefore the method was discarded.

Three-class classification was performed for pepsin concentration, pH, and ionic strength (Table 3.2), grouping pH values ≤ 2 and pepsin concentrations $\geq 310\,\mathrm{U/mL}$ to improve class balance. For the degree of hydrolysis (DH), the final classification layer was replaced by a single output regression node, trained with mean squared error. The output in this case represented the estimated DH difference between the video's starting frame and the following frames. Training was done by selecting a random video, then sampling two frames separated by Δt and randomly manipulate them to augment the training. For DH regression, 12 videos were used. Michaelis-Menten fits (Equation 3.5) were used to assign ground truth DH values. Two frames were sampled from the first and second halves of each video, and the model predicted the DH change. Training was conducted for 200 epochs, selected based on training loss and validation performance to balance overfitting and generalization. Each model required approximately 1 hour to train. For validation, a train/validation split was used for the three-classifier scenario, while full leave-one-out validation was applied for DH regression. In the three-classifier case, three videos per class were used for validation, ensuring a mix of categories, with the rest used for training. For DH regression, each video was used once for validation while training on the remaining data, providing a robust evaluation despite increased training time. For DH classification, each predicted video was validated using a leave-one-out approach across the 12 videos.

For additional details, the reader is referred to the explanation in Manuscript I.

Table 3.2: *Classes used for the classification of the three categories of pepsin concentration, pH, and ionic strength.*

Class	Pepsin concentration (U/mL)	pH	Ionic Strength (mM)
Class 1	0	≤ 2	~ 0
Class 2	150	3	98
Class 3	≥ 310	7	142

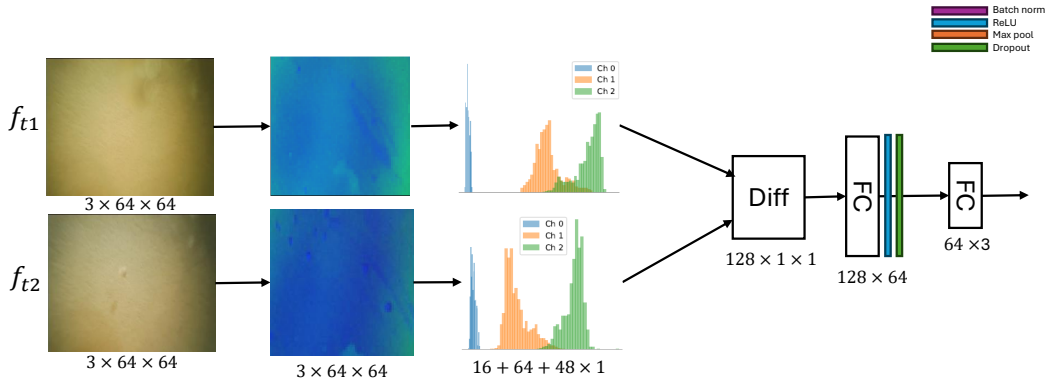

(a)

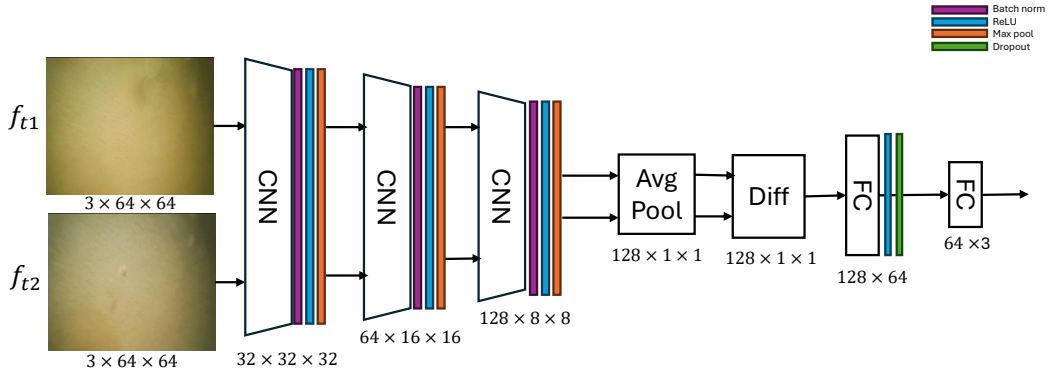

(b)

Figure 3.3: *Architectures of the HSV+MLP (a) and CNN+MLP (b) models. For classification (pH, pepsin concentration, ionic strength), the final layer has three outputs and uses cross-entropy loss. For DH regression, it has a single output and uses mean squared error. All other parameters are identical.*

3.5 *In vitro* human colonic fermentation of pectin

3.5.1 Preparation of medium and inoculum

A 1500 mL medium was prepared by combining basal solution, phosphate buffer, bicarbonate, and vitamins, excluding a carbon source, as described by Karlsson *et al.* [85]. The medium was divided into seven 500 mL Schott bottles, sterilized by autoclaving at 121 °C for 20 min, and anaerobic conditions were established by bubbling with nitrogen for 45 min and adding 1 mL of reducing agent.

Inoculum preparation was performed under sterile conditions in a laminar airflow (LAF) bench. Feces from three human volunteers with unrestricted diets and no gastrointestinal diseases were collected. Samples were diluted to 20 wt% with sterile 50 mM phosphate buffer, homogenized, and filtered to remove solid particles. Inoculum preparation occurred within 2 hours of collection to preserve microbial viability. Each experiment was performed in triplicate, using a separate donor for each run. Ethical guidelines were followed and approved by the Swedish Ethical Review Authority (2022-01696-01).

3.5.2 *In vitro* fermentation

If dispersions, to each substrate, 10 mL of fecal inoculum was added and mixed using a vortex. The mixture was then transferred into bottles containing the anaerobic medium, using a syringe to reach a total volume of 100 mL. If gels, all these steps were done in an anaerobic glovebox. The gel was cut into ∼0.5 cm side cubes, and mixing was applied by hand. The final concentration of dry substrate in each bottle was 1 %. The bottles were incubated at 37 °C for 24 h with stirring, with samples taken at 0, 4, 8, and 24 h. A 24-hour time limit was chosen to minimize metabolite accumulation, as the batch fermentation setup lacks substrate and product influx and efflux. Samples were centrifuged at 4 °C and 18,000 rpm to halt fermentation, and the pellet and supernatant were separated. pH was measured in the supernatant, and samples were stored at -80 °C for further analysis. Total gas production was monitored over time in each bottle using the Gas Endeavor system (BPC Instruments, Sweden), which measures low gas volumes and flow during fermentation. SCFA concentrations (acetate, propionate, butyrate) were measured at 0, 4, 8, and 24 h using UHPLC-qToF-MS following the 3-nitrophenylhydrazine (3-NPH) derivatization method [86], as described by Karlsson *et al.* [85]. A blank containing only the medium and fecal inoculum was also prepared.

4 Results and discussion

4.1 Preparation and characterization of gelatin gels for *in vitro* gastric digestion

The behavior under gastric-like conditions of gelatin gels crosslinked with TGase was investigated. By varying pH, ionic strength, and pepsin concentration, I explored how media conditions, as simplified gastrointestinal environments, modulate gel swelling, enzymatic action, and the overall mechanism of gel digestion. In parallel, an ML-based video analysis approach was employed to predict disappearance and digestion parameters from the gels' visual changes over time.

4.1.1 Enzymatic crosslinking of gelatin gels and their swelling

Small deformation rheology was used to determine gelatin and the TGase-crosslinked gelatin stability at 37 °C, as well as their storage modulus (G') and loss modulus (G''). At 37 °C, gelatin behaves as a liquid with G'' greater than G', consistent with previous findings [37]. Upon addition of TGase, however, gelatin transforms into a visco-elastic semi-solid within 5 minutes, as demonstrated by a rapid increase in storage G' exceeding G'' by two orders of magnitude (Figure 4.1). The melting temperature (T_{m}) of the gel, determined from the crossover of G' and G'' during heating, increased from 34 °C to above 60 °C. In large deformation tests, TGase-crosslinked gels exhibited a 160 % increase in compression stress and a 60 % increase in strain at break compared to gelatin with no TGase (Table 4.1), confirming effective enzymatic crosslinking.

TGase catalyzes covalent bonding between the γ-carboxamide groups of glutamine and ε-amino groups of lysine residues, producing a chemical network that resists melting [87] and allows subsequent analysis at 37 °C.

Swelling behavior was evaluated in media of varying pH, ionic strength, and pepsin content to mimic gastrointestinal conditions. Gelatin type A, with an isoelectric point above pH 7, becomes positively charged in acidic environments [36]. Swelling was greater in salt-free solutions (see Figure 4.2a) and at pH values far from the gelatin pI (see Figure 4.2b), in line with reported enhanced electrostatic repulsion and polymer expansion [43, 88]. As ionic strength

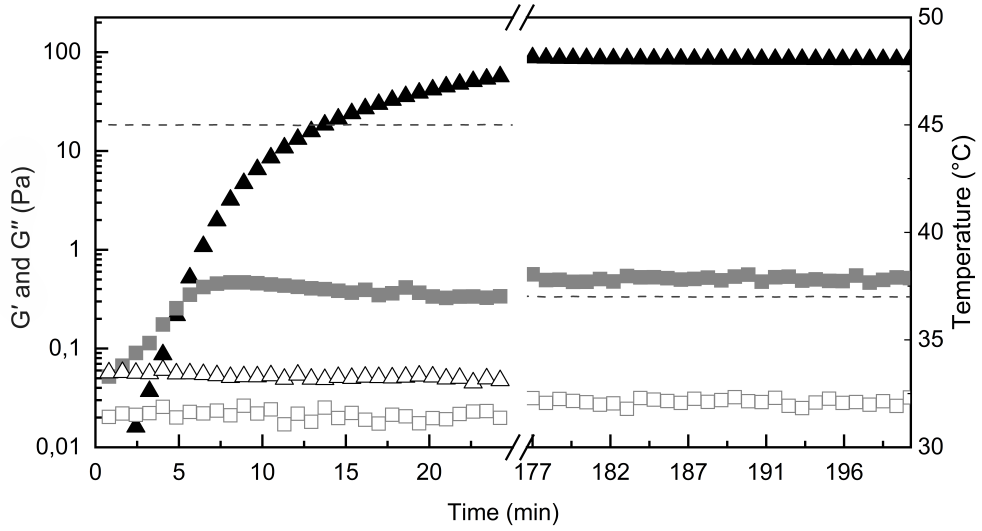

Figure 4.1: *G' (▲) and G'' (■) of gelatin as a function of time with TGase (filled) and without TGase (open) during the activation of TGase at 45 °C (left), and gel behavior at 37 °C (right). Temperature is shown with a dashed line.*

Table 4.1: *Gel properties as defined by small and large deformation of gelatin and TGase-crosslinked gelatin where the stress and strain at break were defined at room temperature.*

Gel properties	Gelatin	Gelatin + TGase
Compression stress at break (kPa)	9.1 ± 3.5	23.4 ± 6.6
Strain at break (mm/mm)	0.6 ± 0.1	0.8 ± 0.0
T_m (°C)	34	> 60
G' at 37 °C (Pa)	<1	84 ± 11
G'' at 37 °C (Pa)	0.03 ± 0.01	0.50 ± 0.06

increased, swelling decreased significantly, likely due to a decrease in chemical potential gradient between the inside of the gel and the surrounding media.

To further characterize the swelling mechanism, data were fitted to an empirical Fickian model (Equation 3.3), with diffusion exponents (n) and constants (k) listed in Table 4.2. At both pH 3 and 7, increasing ionic strength caused n to decrease toward 0.5, indicating a transition toward Fickian (diffusion-controlled) swelling. In contrast, low-salinity media often showed $0.5 < n < 1.0$, suggestive of anomalous or non-Fickian diffusion, where the swelling is not simply diffusion-controlled. Addition of pepsin increased n in both 1.5S and 3S media, possibly due to enzyme-induced changes in network mobility or partial

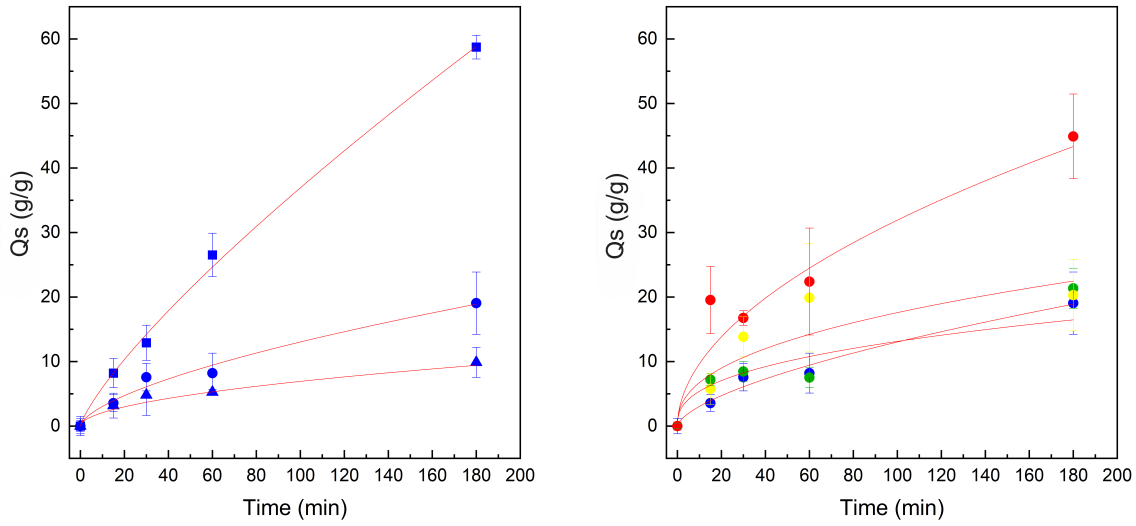

(a) **(b)**

Figure 4.2: *Water uptake (Q_s) of TGase crosslinked gelatin gels as a function of ionic strength at pH 7 (a) and as a function of pH at ionic strength of 98 mM (b). Filled square represent ionic strength of ∼0 mM, filled circle 98 mM, filled triangles 142 mM. Blue represent a pH of 7, green of 3, yellow of 2 and red of 1.5.*

degradation. No consistent n trend was observed across different pH values at constant ionic strength, although in some conditions (e.g., pH 1.5 with pepsin), n values approached 1.0, reflecting non-Fickian behavior.

Table 4.2: *Fick's parameters k and n of the fit obtained from the empirical data measured through gravimetric swelling tests.*

Media's acronym	k	n
70	0.96 ± 0.14	0.79 ± 0.03
7S	0.71 ± 0.23	0.63 ± 0.08
7I	0.62 ± 0.16	0.52 ± 0.06
30	3.8 ± 0.3	0.61 ± 0.02
3S	2.2 ± 1.3	0.39 ± 0.02
3I	0.97 ± 0.52	0.30 ± 0.00
3Spb	1.0 ± 0.4	0.50 ± 0.10
2S	2.6 ± 1.4	0.42 ± 0.13
1.5S	2.9 ± 0.9	0.52 ± 0.07
1.5Spb	0.80 ± 0.38	0.73 ± 0.16

Overall, TGase crosslinking significantly increased the mechanical and thermal stability of gelatin. Furthermore, the resistance of the TGase gelatin gels enables

us to analyze swelling and digestion and to record videos long enough for further processing with ML models.

4.1.2 Gelatin gel digestion and disappearance

The degradation of TGase-crosslinked gelatin gels was assessed using pepsin as a representative gastric enzyme. No visible disintegration was observed in the absence of pepsin, even under acidic conditions. Upon the addition of pepsin, the degree of hydrolysis (DH) reached approximately 20 % at pH 1.5 and 2, and around 10 % at pH 3 (Figure 4.3). Complete gel disappearance occurred between 20 and 170 minutes, depending on the pH. These DH values, and the pH-dependence of pepsin activity, align with previously reported data [89, 90]. In contrast, gels exposed only to low-pH conditions (without pepsin) exhibited DH values below 2 %, confirming that enzymatic activity, rather than acid-induced hydrolysis, is the dominant mechanism of gel breakdown.

For ML analysis based on time-resolved video, it is essential that the gel remains anchored to the camera probe throughout the observation period. Tests across varying pH and ionic strength confirmed that swelling alone does not lead to detachment or disintegration. Only in the presence of pepsin was visual degradation observed, leading to eventual detachment from the probe. This supports the conclusion that enzymatic hydrolysis, not swelling, governs gel collapse under gastric-like conditions.

Although pepsin is broadly proteolytic, it preferentially cleaves peptide bonds adjacent to aromatic amino acids (AAAs) such as tyrosine (Tyr), phenylalanine (Phe), and tryptophan (Trp). Type A gelatin derived from porcine skin contains approximately 3.9 % AAAs and lacks Trp [91, 92], which may limit the extent of proteolysis. This is reflected in the maximum DH values observed (Figure 4.3), which plateau at ∼20 % under optimal acidic conditions (pH 1.5-2) and decrease to ∼10 % at pH 3. Pepsin activity exhibited a clear pH dependence, with maximal activity near pH 2 and significantly reduced efficacy at pH 3.

4.1.3 Evaluation of machine learning models in video analysis of *in vitro* gelatin digestion conditions

ML models were trained to analyze time-resolved video frames of gelatin gels undergoing digestion and to predict the conditions in the digestion media. Figure 4.4 shows the *predicted versus actual change in DH* relative to the first video frame for the samples at pH 3 and ionic strength of 98 mM. Briefly, the green and yellow lines represent the predictions of the two models, which are ideally expected to closely align with the blue line, corresponding to the actual DH measurements. Across 12 videos, the CNN+MLP model achieved an average root mean square error (RMSE) of 3.29 ± 2.30, outperforming the HSV+MLP model

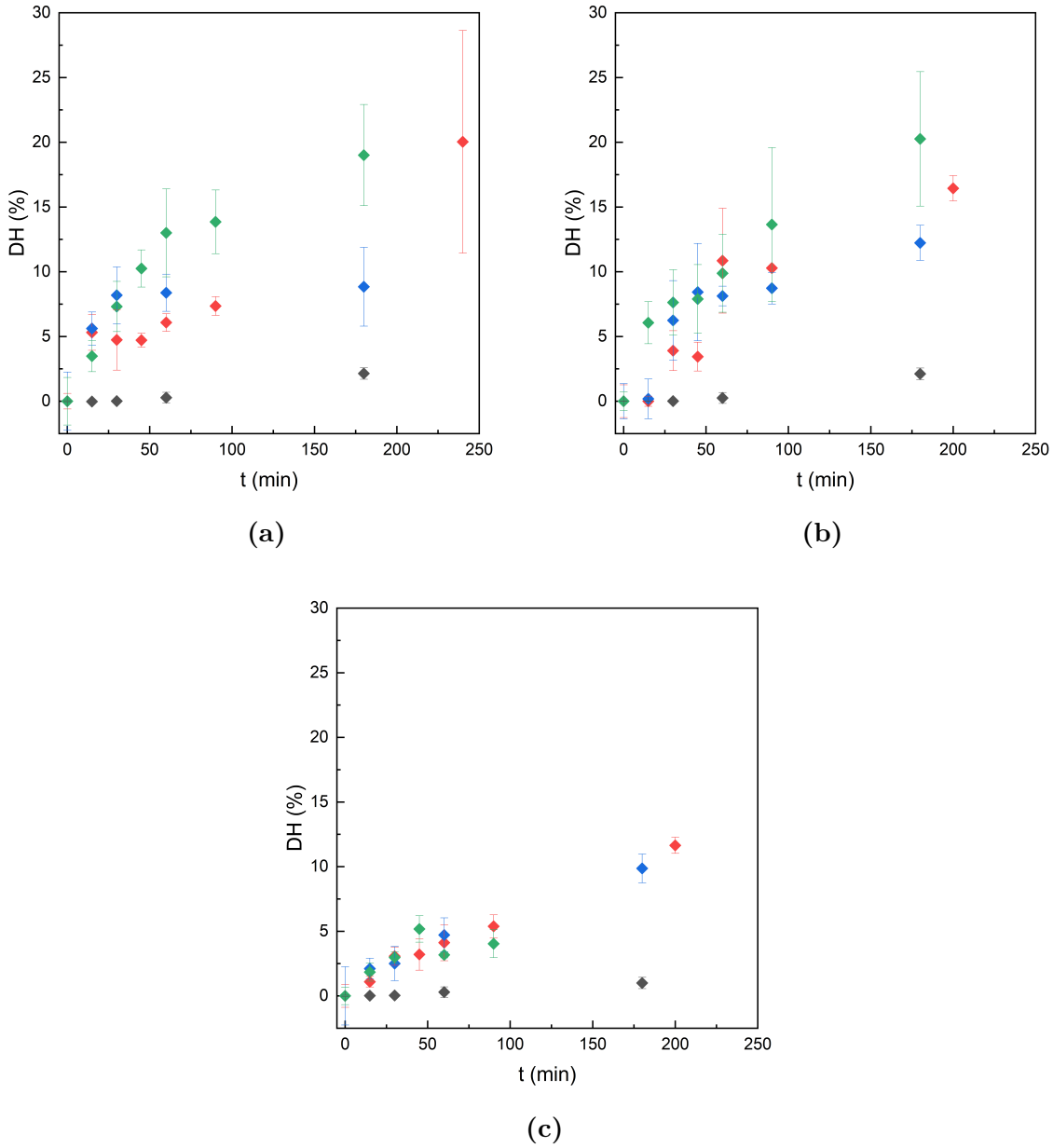

Figure 4.3: *DH of gelatin as a function of time and concentration of pepsin and media pH of 1.5 (a), pH 2 (b), and pH 3 (c), where black symbols represent no addition of pepsin, red symbols the addition of 150, blue symbols of 310, and green symbols of 750 U/ml. The media ionic strength is fixed at 98 mM.*

with an RMSE of 3.44 ± 2.05. Notably, the CNN+MLP model produced RMSE values below 2.0 for 6 of the 12 videos, compared to only 3 for the HSV+MLP, indicating higher robustness in learning spatial features correlated with DH. Both models were trained on the full video duration, although relevant digestion events may occur within a narrower temporal window. The model architecture enabled

it to capture complex visual cues associated with enzymatic breakdown. The isolated spikes in the prediction lines correspond to moments when the neutral booth was opened for digesta sampling, briefly exposing the setup to ambient light and causing erroneous model predictions.

In the classification task, better performances for both models across all three classification categories were achieved with a higher temporal difference (Δt) between the frames. Specifically, at a Δt of 60 minutes, with the exception of HSV+MLP for pepsin concentration, which performed best at $\Delta t = 50$ minutes. This reflects a trade-off between prediction speed and accuracy, as longer Δt values enhance model performance by capturing more pronounced gel degradation, especially during phases of rapid breakdown.

CNN+MLP yielded the highest accuracy for pH and ionic strength classification, while HSV+MLP performed best for pepsin concentration. This is attributed to the pronounced color saturation changes induced by enzymatic activity, which are directly captured by the HSV representation. In contrast, CNNs leverage spatial and textural patterns, enabling better discrimination of subtler features such as pH-induced swelling or ionic strength effects.

Confusion matrices (Table 4.3) reveal that misclassifications tended to occur between adjacent or visually similar classes, for example, between pH 3 and pH $\leq$ 2, or between ionic strengths of 98 and 142 mM. Pepsin concentration classification showed minimal confusion between 0 and $\geq$ 310 U/mL, suggesting a reliable distinction between no digestion and intense enzymatic action. This highlights a higher sensitivity of the models to enzyme-induced digestion over physiological parameters alone, since in pepsin-free conditions, videos displayed only minor color shifts and no gel disappearance.

Overall, the CNN+MLP model demonstrated better generalization and predictive power, showing that spatial feature differences detection could outperform HSV color metrics in this study. The model architectures also support classification and regression tasks, offering a broad framework for analyzing *in vitro* and potentially *in vivo* digestion via visual input.

Table 4.3: *Confusion matrices (%) for a leave-one-out validation for the best model at classifying pepsin (a), pH (b), and ionic strength (c). Rows are true class, and columns are predicted class.*

Pepsin conc. (U/mL)	0	150	≥ 310
0	66.7	33.3	0.0
150	5.6	60.0	34.4
≥ 310	10.0	33.3	56.7

(a)

pH	≤ 2	3	7
≤ 2	70.0	30.0	0.0
3	66.7	27.8	5.6
7	0.0	88.3	11.7

(b)

Ionic strength (mM)	~ 0	98	142
~ 0	68.6	31.4	0.0
98	7.8	34.4	57.8
142	61.1	3.3	35.6

(c)

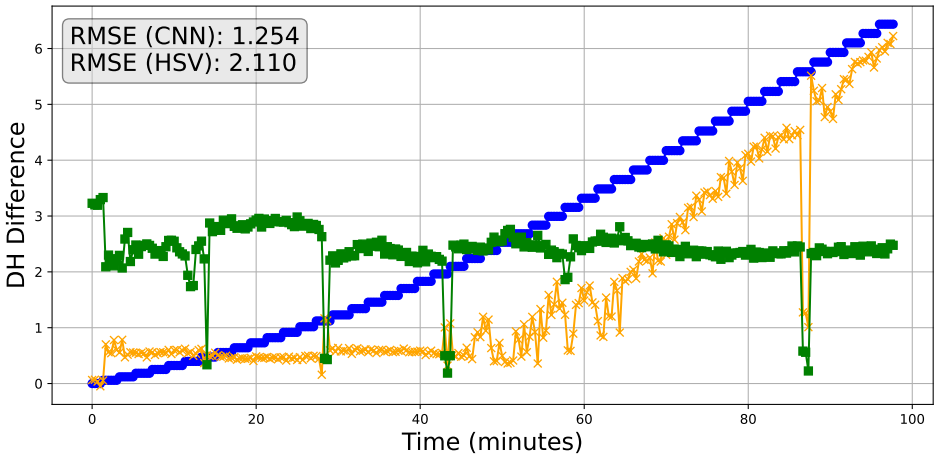

(a)

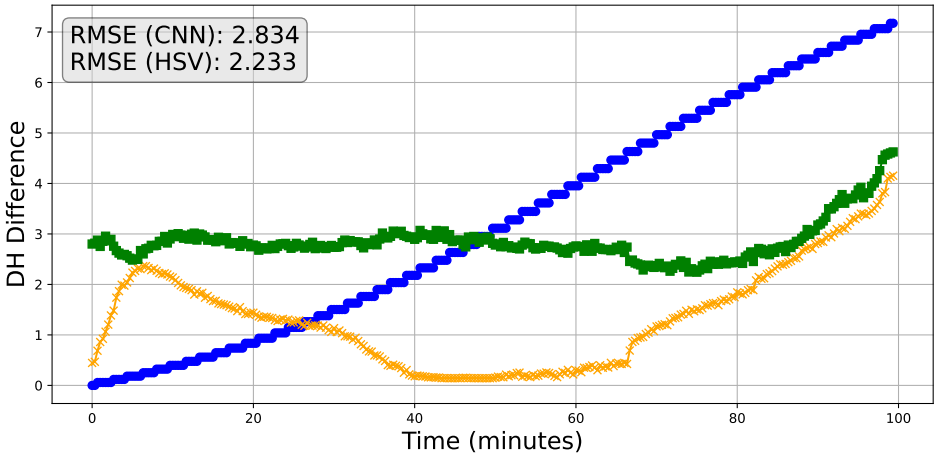

(b)

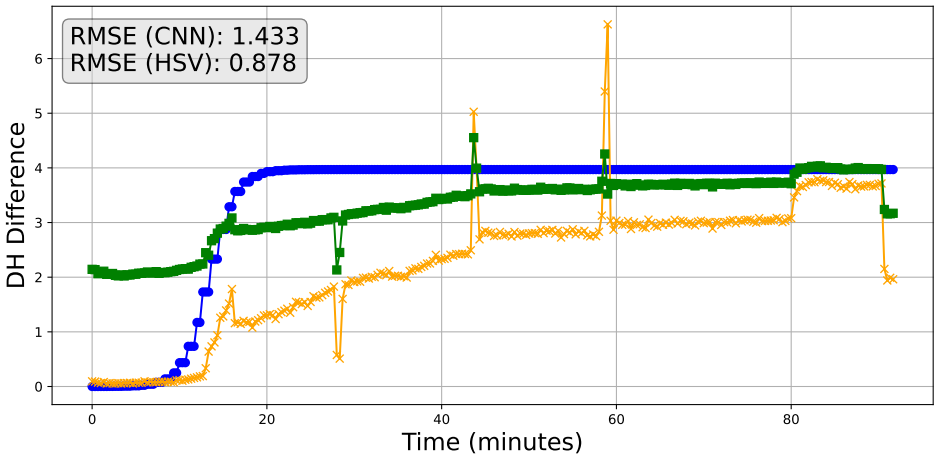

(c)

Figure 4.4: *Predicted change in degree of hydrolysis (DH) for the HSV+MLP model (green), CNN+MLP model (orange), and actual change in DH (blue) from the first frame and all other frames for 3 out of 12 videos: 3Spa (a), 3Spb (b) and 3Spc (c).*

4.2 Preparation and characterization of PGA and pectin gels for *in vitro* colonic fermentation

This section examines how chemical modifications, partial methylation, and alkaline hydrolysis affect the physicochemical properties, gelation behavior, and fermentability of pectin and PGA. Changes in molar mass, viscosity, and calcium-induced gel structure were characterized, while fermentability was assessed using an *in vitro* colonic model comparing pectin in dispersion and gel form.

4.2.1 Degree of methylation and molar mass of PGA and pectin

The FTIR spectra of the powders show a clear change in the intensity of the peak at 1736 cm^{-1} as reaction time progresses. The degree of methylation (DM) was calculated from the FTIR spectra using Equation 3.1.

PGA methylation yielded DM values of 11 %, 26 %, and 35 % for reaction times of 1, 5, and 10 days, respectively, thus they were labeled as MeO-PGA-11, MeO-PGA-26, and MeO-PGA-35, corresponding to their DM values. SEC-MALS was employed to monitor the changes in the number and weight average molar mass, since the methylation reaction is known to degrade the polymer through β-elimination occurring on the PGA backbone [75, 93]. As shown in Table 4.4, despite the cold conditions, which slow the rate of β-elimination hydrolysis, a decrease in M_{w} and M_{n} was observed anyway, proportional to reaction time. The PGA with the highest DM nearly halved its molar mass by the end of the reaction. The intrinsic viscosity ($[\eta]$), obtained from SEC with an IV detector, followed the same reduction trend as M_{w} and M_{n}, corroborating the results from the MALS detector. Mass recoveries of the injected volume were 88%, 85%, 75%, and 86% for PGA, MeO-PGA-11, MeO-PGA-26, and MeO-PGA-35, respectively.

Hydrolyzed pectin exhibited a clear decrease in DM, dropping from 32 % in the original pectin to 25 % after 24 hours of reaction. This reduction reflects the action of alkaline hydrolysis on the PGA backbone, which proceeds via the β-elimination mechanism previously described. In addition to backbone cleavage, side chains may also be removed through alkaline de-esterification during the reaction [94]. Consistent with these structural modifications, chemical hydrolysis also led to a reduction in the polymers molar mass and $[\eta]$.

4.2.2 Viscosity of PGA and pectin dispersions

The effect of methylation and hydrolysis on PGA and pectin solution properties was evaluated via rheology and small-angle neutron scattering (SANS) performed

Table 4.4: *Degree of methylation (DM), molar mass, and intrinsic viscosity ([η]) of pectins, PGA, and MeO-PGA obtained from SEC-MALS-IV. M_n stands for the number-averaged molar mass, M_w for the weight-averaged molar mass, $Đ_M$ is the molar mass dispersity.*

Samples	DM (%)	$\overline{M_n}$ (kDa)	$\overline{M_w}$ (kDa)	$Đ_M \left(\frac{\overline{M_w}}{\overline{M_n}}\right)$	[η] (mL/g)
Pectin	32	104 ± 1	289 ± 11	2.8	230 ± 29
Hydrolyzed pectin	25	108 ± 9	221 ± 14	2.0	200 ± 11
PGA	0	45 ± 6	117 ± 5	2.6	305 ± 6
MeO-PGA-11	11	57 ± 9	103 ± 5	1.8	232 ± 6
MeO-PGA-26	26	24 ± 2	82 ± 3	3.4	219 ± 9
MeO-PGA-35	35	24 ± 1	63 ± 3	2.6	180 ± 13

in collaboration with Dr. Cousin at CEA, France. For PGA and MeO-PGA, two concentration regimes were observed, dilute and semi-dilute, with the overlap concentration C^* increasing with DM: from 11.5 g/L (PGA, MeO-PGA-11) to 15.0 g/L (MeO-PGA-35), reflecting reduced chain overlap with increasing methylation (see Figure 4.5a). Despite this, methylation did not affect the polymer-solvent interaction significantly, as the slope of the master curve apparent viscosity vs. $C[\eta]$ plots remained 1.2 across all samples (see Figure 4.5b). Finally, SANS data showed that aggregation was comparable across PGA and MeO-PGA. Persistence lengths L_p were estimated to be 80 Å for native PGA, and increased with DM (from 58 Å at DM 11 % to 84 Å at DM 35 %).

Alkaline hydrolysis led to a substantial decrease in the viscosity of 3 % pectin solutions, from 1,551 mPas to 95 mPas. This marked reduction can be attributed to both the loss in molar mass and the decrease in DM (Table 4.4).

Overall, methylation stiffens PGA chains and shifts C^* upward, while reducing molar mass through chain scission; besides, alkaline hydrolysis also reduces molar mass through the same mechanism, and reduces the dispersion's viscosity. Aggregates in SEC-MALS were excluded through solution preparation steps, confirming that property changes reflect intrinsic structural modifications. For further details on SANS, refer to Manuscript II.

4.2.3 Gelation and properties of calcium-induced PGA gels

Visual examination of the PGA and MeO-PGA calcium-based hydrogels (DM = 0 %, 11 %, 26 %, 35 %) revealed distinct differences in appearance (see Figure 4.6). PGA hydrogels were fully transparent, in agreement with previous findings, whereas increasing DM resulted in progressively turbid gels. The observed turbidity was uniform throughout each gel, indicating homogeneous mesoscopic heterogeneities across the sample, including regions closest to the

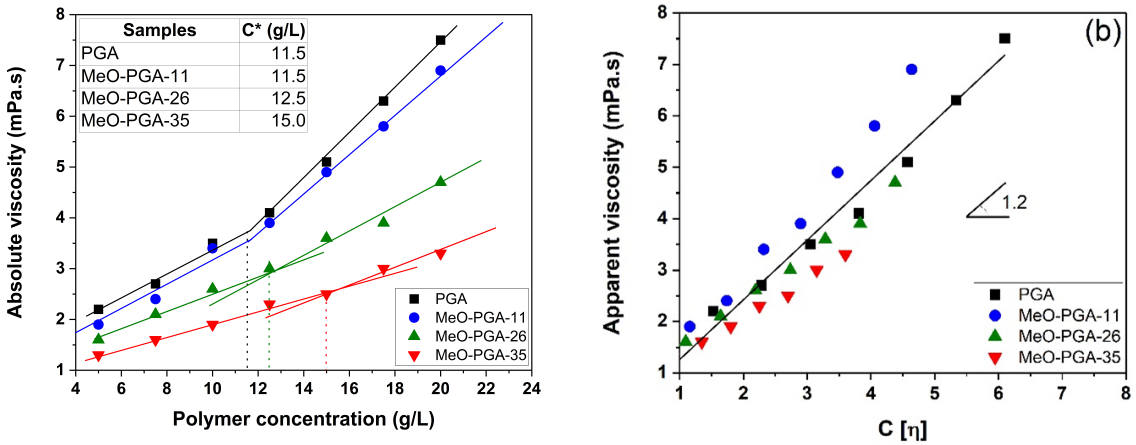

Figure 4.5: *Absolute viscosity as a function of polymer concentration (a) at a shear rate of 20 s^{-1}, and apparent viscosity of the samples plotted against the degree of coil overlap (b), characterized by $C[\eta]$, where $[\eta]$ is the intrinsic viscosity determined by SEC-MALS. The samples are solutions of PGA (black), MeO-PGA-11 (blue), MeO-PGA-26 (green), and MeO-PGA-35 (red).*

calcium reservoir. This behavior contrasts with Zn(II)- and Fe(II)-PGA hydrogels [95], where a turbidity gradient was observed due to progressive heterogeneity development along the gel height, linked to the stronger monodentate egg-box associations specific to Zn^{2+} and Fe^{2+} coordination.

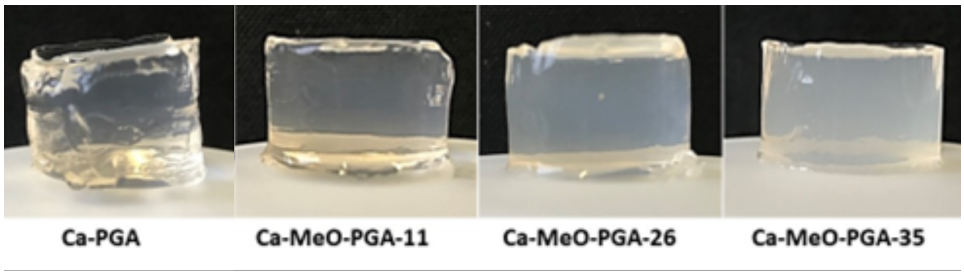

Figure 4.6: *Picture of the Ca-PGA hydrogel and the three Ca-MeO-PGA hydrogels.*

To further understand the gel structure, hydrogels were sliced and individually analyzed with SANS, performed through collaborations, which confirmed that crosslinking occurred. Mesh size (ξ) was obtained by using an Ornstein-Zernike structure factor (see Table 4.5). For DM = 0 %, ξ was comparable to the chain persistence length L_p, suggesting tight, stiffness-constrained networks. This is likely due to the shorter spacing between egg-box junctions, as the polymer backbone is fully available for calcium crosslinking. In contrast, methylation led to larger mesh sizes, with ξ/L_p increasing to 1.7 at DM = 35 %, reflecting reduced crosslinking density due to fewer neighboring carboxylate groups available to form

egg-box junctions, and a fivefold increase in mesh volume. For further details on SANS, refer to Manuscript II.

Table 4.5: *Mesh size (ξ) of the first slice and persistence length (L_p) at 5 g/L of PGA and MeO-PGA samples, as obtained in Manuscript II.*

	DM	DM 11 %	DM 26 %	DM 35 %
L_p (Å)	80	58	64	84
ξ (Å)	80	80	110	140
ξ / L_p	1.0	1.4	1.7	1.7

4.2.4 Impact of molar mass on pectin *in vitro* colonic fermentation

Although no major differences were observed in the relative composition of SCFAs, the total SCFA production was significantly higher at later times for the hydrolyzed pectin compared to the untreated counterpart (Figure 4.7c). These results suggest that alkaline hydrolysis may enhance the fermentability of pectin, potentially by reducing molar mass and improving accessibility to microbial metabolic pathways, as previously observed in literature [96, 97]. While only a single hydrolysis condition was tested, future studies will be needed to confirm and expand on these findings by systematically varying hydrolysis time and severity. Notably, several studies have shown that the DM influences the fermentability of pectins, although findings are often contradictory with each other [98–100].

Regarding pH evolution, the buffering capacity typically conferred by $-$COOH groups was diminished in the hydrolyzed sample (Figure 4.7b). Nevertheless, all samples eventually reached comparable final pH values during fermentation. Similarly, despite the wide standard deviation, gas production profiles were similar between the two samples (Figure 4.7a), indicating that the overall extent of microbial activity was not substantially affected by the hydrolysis, but rather their metabolic pathways.

4.2.5 Impact of gelation on pectin *in vitro* colonic fermentation

Previous studies have reported that gelled form of polysaccharide ferment more slowly than their corresponding dispersions, where gel particle size and polymer type influence the rate of fermentation [68]. Notably, pectin particles from around 0.5 mm and above were found to ferment similarly to pectin solutions, suggesting a threshold, below which gel structure no longer impedes microbial access. In contrast, my results show that 3 % calcium-crosslinked pectin gels

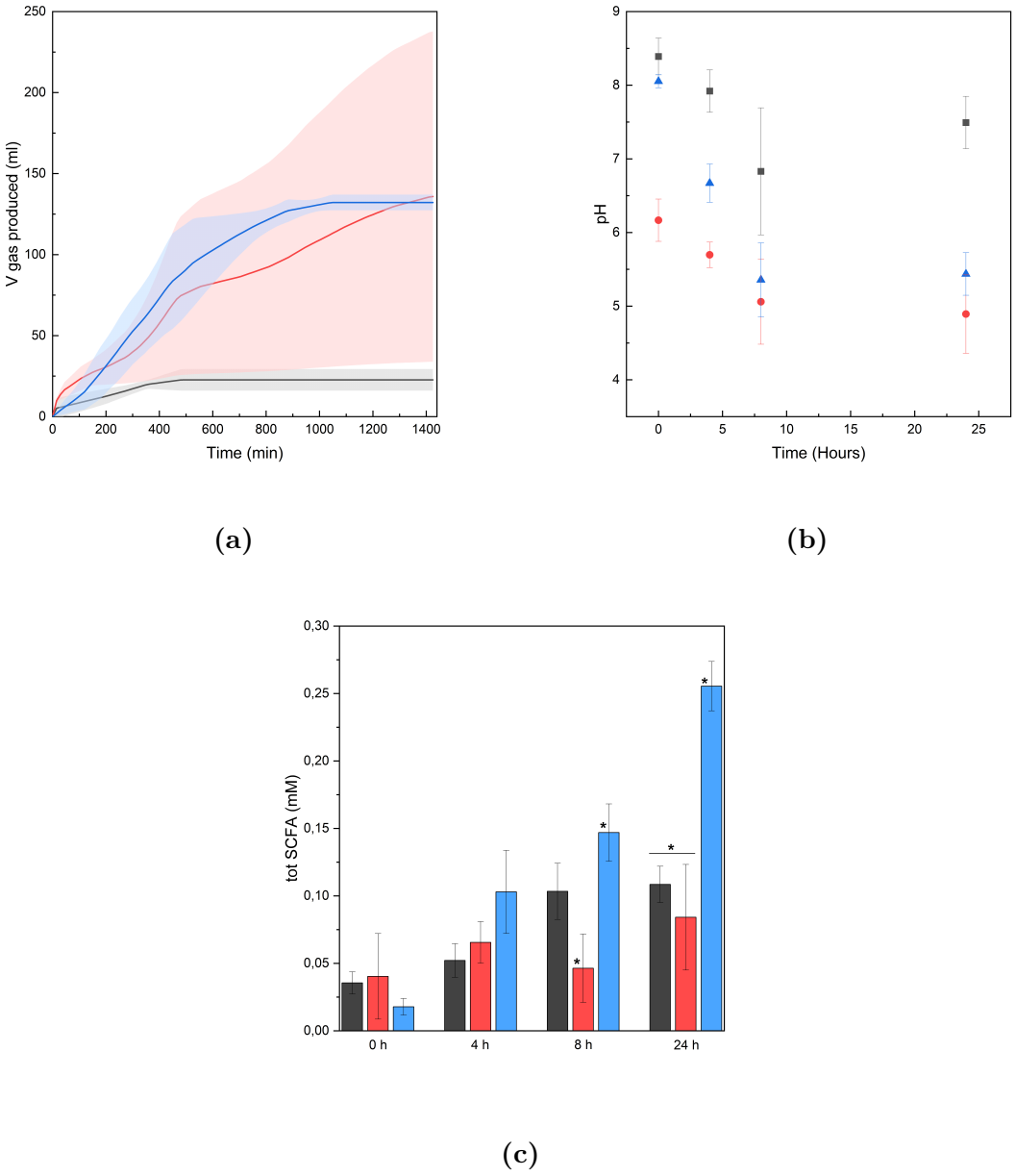

Figure 4.7: *Gas production (a), pH change (b), and total SCFA production (c) of pectin dispersions of the native pectin (red) and the hydrolyzed (blue). Control is in black. * indicates statistical difference.*

produced higher total SCFA levels at later times than their dispersion counterparts (Figure 4.8c), despite similar SCFA composition and gas production (Figure 4.8a). This divergence may be attributed to differences in gel structure, GDL introduced during gelation, or the bigger gel particle size used in this study (∼0.5 cm side cubes). Additionally, the pH evolution was comparable across both forms (Figure 4.8b), indicating that the buffering capacity of pectin remained consistent

regardless of its physical state. These findings suggest that, under certain conditions, gelation may enhance rather than hinder fermentability, challenging previous assumptions and underscoring the need for further investigation into how gel structure and composition modulate microbial activity.

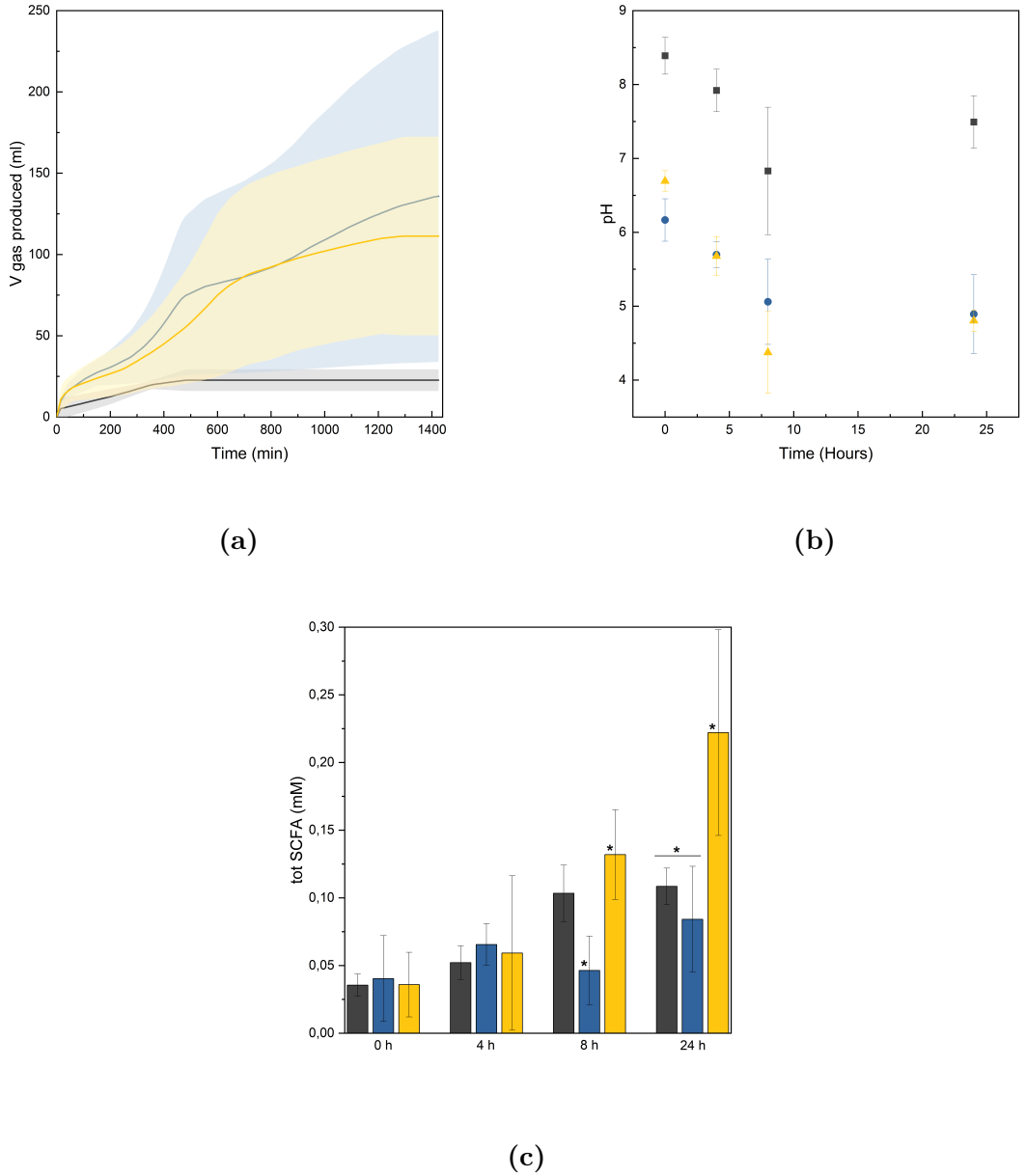

(a) **(b)**

(c)

Figure 4.8: *Gas production (a), pH change (b), and total SCFA production (c) of pectin dispersion (blue) and gel obtained by GDL + $CaCO_3$ (yellow). Control is in black. * indicates statistical difference.*

5 Conclusions and future work

In this thesis, I presented the possibility of applying ML tools to evaluate digestion conditions. To achieve this, I developed an *in vitro* system to reliably capture the degradation of gelatin gels on video, enabling the collection of relevant data for ML analysis (see Figure 3.2). I have shown that ML, particularly CNN+MLP models, can effectively predict the DH and classify digestive conditions such as pepsin concentration, pH, and ionic strength, using solely visual cues.

I have successfully studied gelatin behavior in digestive environments, underscoring the role of TGase in crosslinking gelatin gels, preventing dissolution at body temperature. The swelling behavior of the gels was influenced by both pH and ionic strength, with maximum swelling occurring in salt-free conditions and at pH values distant from gelatins isoelectric point. Adding pepsin further altered the swelling dynamics by potentially increasing chain mobility and promoting gel breakdown. This indicates that enzymatic hydrolysis, rather than osmotic swelling, is the primary mechanism responsible for gel collapse under gastric-like conditions. Furthermore, the yellow dye was a functional integration for color-based ML analysis.

I investigated properties of pectin and PGA, showing that methylation increased DM, reduced molar mass, and raised overlap concentration, while hydrolysis decreased both DM and viscosity. In calcium-crosslinked hydrogels, methylation led to higher turbidity and mesh size, reducing crosslinking density. Using an *in vitro* human colonic fermentation model, I found that hydrolyzed pectin produced more total SCFAs than untreated pectin, though SCFA composition profiles and gas production were similar. Gelled pectin generated more SCFAs than dispersed pectin, likely due to structural differences and perhaps the presence of GDL as a carbon source.

My work supports the hypothesis stated and demonstrates the potential of integrating imaging tools with ML into the analysis of *in vitro* digestion. A robust method was established to capture video data, coat probes, and control gel conditions, laying the groundwork for future ML applications. The following steps will involve refining these models and expanding them to polysaccharides, including blended systems of pectin and gelatin, to better predict their digestion and gut fermentation.

Acknowledgments

I would like to express my deepest gratitude to my supervisor, Anna Ström, for her kindness, and to my co-supervisor, Patricia López-Sánchez, for her openness. Both of them, along with their endless patience and thoroughness, have guided me throughout this journey.

Thanks also to my examiner, Martin Andersson, and my director of studies, Ergang Wang, for their supervision; and to my discussion leader, Romain Bordes, thank you for your time and insight. I am grateful as well to my collaborators, particularly Martin Längkvist and Tatiana Marques, for their valuable input along the way. I also gratefully acknowledge Chalmers University of Technology for financial support.

Now to the boys, Jakob, Leo, and Eliott. Thank you for the great time, and making Chalmers a lighter place. Hugs to Judith, Eva, Monika, Ehsan, Maja, Elin and the whole Applied Chemistry team for the chats, the climbs, and the good company.

To the Chemical Engineering team, and Phuoc among them all: if I'm still here is thanks to your striking drive. Shout-out to Juan and her seamless energy in helping me make my life feel less scattered. Big thanks to my kompisar, Julia, Lore and Leo, that made the SFI shenanigans less traumatic. To my D&D crew, Victor, Nick, Nicolas, Sigma, Jesus and Margit: thank you for the mental voyages, from Göteborg to far-off fantasy lands; they are just priceless. A heartfelt thank you to the Poppi gang, Elia, Davide and Alessandro, and to my family, mom, dad and Franci, always at the other end of the phone. You are my deepest roots, stretching all the way to Italy.

Lastly, to Moa: thank you for the invaluable love and support you give me everyday. Looking forward to more of our train odysseys, heart-warming bonfires and sweet Swedish lessons. None of this would have been the same without you.

References

[1] *Physiology of the Gastrointestinal Tract*, 6th ed.; Said, H. M., Ed.; Academic Press: 2018.

[2] Sekirov, I.; Russell, S. L.; Caetano M Antunes, L.; Finlay, B. B. Gut microbiota in health and disease. *Physiological Reviews* **2010**, *90*, 859 –904.

[3] Eussen, S. R.; Verhagen, H.; Klungel, O. H.; Garssen, J.; van Loveren, H.; van Kranen, H. J.; Rompelberg, C. J. Functional foods and dietary supplements: Products at the interface between pharma and nutrition. *European Journal of Pharmacology* **2011**, *668*, S2–S9.

[4] *Nutrition and Functional Foods for Healthy Aging*; Watson, R. R., Ed.; Academic Press: 2017.

[5] Saltzman, J. R.; Russell, R. M. The Aging Gut: Nutritional Issues. *Gastroenterology Clinics of North America* **1998**, *27*, 309–324.

[6] Monteiro, M. P.; Batterham, R. L. The Importance of the Gastrointestinal Tract in Controlling Food Intake and Regulating Energy Balance. *Gastroenterology* **2017**, *152*, 1707–1717.

[7] Nadia, J.; Roy, D.; Montoya, C. A.; Singh, H.; Acevedo-Fani, A.; Bornhorst, G. M. A proposed framework to establish in vitro-in vivo relationships using gastric digestion models for food research. *Food Funct.* **2024**, *15*, 10233–10261.

[8] In *The Impact of Food Bioactives on Health: in vitro and ex vivo models*, Verhoeckx, K., Cotter, P., López-Expósito, I., et al., Eds.; Springer: Cham (CH), 2015; Chapter 4.

[9] Sakamoto, H.; Kumazawa, Y.; Motoki, M. Strength of Protein Gels Prepared with Microbial Transglutaminase as Related to Reaction Conditions. *Journal of Food Science* **1994**, *59*, 866 –871.

[10] Willats, W. G. T.; McCartney, L.; Mackie, W.; Knox, J. P. Pectin: Cell biology and prospects for functional analysis. *Plant Molecular Biology* **2001**, *47*, 9–27.

[11] Powell, D.; Morris, E.; Gidley, M.; Rees, D. Conformations and interactions of pectins: II. Influence of residue sequence on chain association in calcium pectate gels. *Journal of Molecular Biology* **1982**, *155*, 517–531.

[12] Bagal-Kestwal, D. R.; Pan, M.; Chiang, B.-H. In *Bio Monomers for Green Polymeric Composite Materials*; John Wiley & Sons, Ltd: 2019; Chapter 6, 117–140.

[13] Ogobuiro, I.; Gonzales, J.; Shumway, K. R., et al., *Physiology, Gastrointestinal*; StatPearls [Internet]; StatPearls Publishing: Treasure Island (FL), 2025.

[14] Somaratne, G.; Ferrua, M. J.; Ye, A.; Nau, F.; Floury, J.; Dupont, D.; and, J. S. Food material properties as determining factors in nutrient release during human gastric digestion: a review. *Critical Reviews in Food Science and Nutrition* **2020**, *60*, 3753–3769.

[15] Rao, M. B.; Tanksale, A. M.; Ghatge, M. S.; Deshpande, V. V. Molecular and Biotechnological Aspects of Microbial Proteases. *Microbiology and Molecular Biology Reviews* **1998**, *62*, 597–635.

[16] Fenna Hinssen Marco Mensink, T. H.; van der Wielen, N. Impact of aging on the digestive system related to protein digestion in vivo. *Critical Reviews in Food Science and Nutrition* **2024**, *0*, 1–17.

[17] Sensoy, I. A review on the food digestion in the digestive tract and the used in vitro models. *Current Research in Food Science* **2021**, *4*, 308–319.

[18] Rothenbuhler, E.; Kinsella, J. E. The pH-stat method for assessing protein digestibility: an evaluation. *Journal of Agricultural and Food Chemistry* **1985**, *33*, 433–438.

[19] Brodkorb, A. et al. INFOGEST static in vitro simulation of gastrointestinal food digestion. *Nature Protocols* **2019**, *14*, 991–1014.

[20] Barroso, E.; Cueva, C.; Peláez, C.; Martínez-Cuesta, M. C.; Requena, T. In *The Impact of Food Bioactives on Health: in vitro and ex vivo models*; Springer International Publishing: Cham, 2015, 319–327.

[21] Van de Wiele, T.; Van den Abbeele, P.; Ossieur, W.; Possemiers, S.; Marzorati, M. In *The Impact of Food Bioactives on Health: in vitro and ex vivo models*; Springer International Publishing: Cham, 2015, 305–317.

[22] Bohn, T. et al. Correlation between in vitro and in vivo data on food digestion. What can we predict with static in vitro digestion models? *Critical Reviews in Food Science and Nutrition* **2018**, *58*, 2239–2261.

[23] Smith, J. R.; Bolton, E. R.; Dwinell, M. R. In *Rat Genomics*; Springer New York: New York, NY, 2019, 1–41.

[24] Miller, E. R.; Ullrey, D. E. The Pig as a Model for Human Nutrition. *Annual Review of Nutrition* **1987**, *7*, 361–382.

[25] Fernandez, M. L.; Volek, J. S. Guinea pigs: A suitable animal model to study lipoprotein metabolism, atherosclerosis and inflammation. *Nutrition & Metabolism* **2006**, *3*, 17.

[26] Veintimilla-Gozalbo, E.; Asensio-Grau, A.; Calvo-Lerma, J.; Heredia, A.; Andrés, A. In Vitro Simulation of Human Colonic Fermentation: A Practical Approach towards Models Design and Analytical Tools. *Applied Sciences* **2021**, *11*.

[27] Costa, C. M.; de Carvalho, N. M.; de Oliveira, D. L.; Madureira, A. R. A Critical Review on In Vitro and Ex Vivo Models of the Intestinal Epithelium of Humans and Monogastric Animals. *Gastrointestinal Disorders* **2024**, *6*, 337–358.

[28] Antal, O.; Dalmadi, I.; Takács, K. Upgrading In Vitro Digestion Protocols with Absorption Models. *Applied Sciences* **2024**, *14*.

[29] Rather, J. A.; Akhter, N.; Ashraf, Q. S.; Mir, S. A.; Makroo, H. A.; Majid, D.; Barba, F. J.; Khaneghah, A. M.; Dar, B. A comprehensive review on gelatin: Understanding impact of the sources, extraction methods, and modifications on potential packaging applications. *Food Packaging and Shelf Life* **2022**, *34*, 100–945.

[30] Roman-Benn, A.; Contador, C. A.; Li, M.-W.; Lam, H.-M.; Ah-Hen, K.; Ulloa, P. E.; Ravanal, M. C. Pectin: An overview of sources, extraction and applications in food products, biomedical, pharmaceutical and environmental issues. *Food Chemistry Advances* **2023**, *2*, 100–192.

[31] Kaya, M.; Sousa, A. G.; Crépeau, M.-J.; Sørensen, S. O.; Ralet, M.-C. Characterization of citrus pectin samples extracted under different conditions: influence of acid type and pH of extraction. *Annals of Botany* **2014**, *114*, 1319–1326.

[32] Haug, I.; Draget, K., *Gelatin*, 2009, 142 –163.

[33] Eastoe, J.; Leach, A. Chemical constitution of gelatin [From mammals, chicken tendon, calf skin, pig skin]. **1977**.

[34] Baydin, T.; Aarstad, O. A.; Dille, M. J.; Hattrem, M. N.; Draget, K. I. Long-term storage stability of type A and type B gelatin gels: The effect of Bloom strength and co-solutes. *Food Hydrocolloids* **2022**, *127*, 107–535.

[35] In *Gelatine Handbook*; John Wiley & Sons, Ltd: 2007; Chapter 2, 45–117.

[36] Tseng, C.-L.; Chen, K.-H.; Su, W.-Y.; Lee, Y.-H.; Wu, C.-C.; Lin, F.-H. Cationic Gelatin Nanoparticles for Drug Delivery to the Ocular Surface: In Vitro and In Vivo Evaluation. *Journal of Nanomaterials* **2013**, *2013*, 238–351.

[37] Reinhard Schrieber, D. H. G. In *Gelatine Handbook*; John Wiley & Sons, Ltd: 2007; Chapter 3, 119–299.

[38] Campiglio, C. E.; Contessi Negrini, N.; Farè, S.; Draghi, L. Cross-Linking Strategies for Electrospun Gelatin Scaffolds. *Materials* **2019**, *12*.

[39] Zambuto, S. G.; Kolluru, S. S.; Ferchichi, E.; Rudewick, H. F.; Fodera, D. M.; Myers, K. M.; Zustiak, S. P.; Oyen, M. L. Evaluation of gelatin bloom strength on gelatin methacryloyl hydrogel properties. *Journal of the Mechanical Behavior of Biomedical Materials* **2024**, *154*, 106–509.

[40] Bloom, O. T. Machine for testing jelly strength of glues, gelatins, and the like, 1925.

[41] Krishnamurti, K. Mechanism of the Swelling of Gels. *Nature* **1929**, *123*, 242–243.

[42] Vigata, M.; Meinert, C.; Bock, N.; Dargaville, B. L.; Hutmacher, D. W. Deciphering the Molecular Mechanism of Water Interaction with Gelatin Methacryloyl Hydrogels: Role of Ionic Strength, pH, Drug Loading and Hydrogel Network Characteristics. *Biomedicines* **2021**, *9*, 574.

[43] Qiao, C.; Cao, X.; Wang, F. Swelling Behavior Study of Physically Crosslinked Gelatin Hydrogels. *Polymers and Polymer Composites* **2012**, *20*, 53–58.

[44] Bergström, S. Estimation of proteolytic activity at mouse implantation sites by the gelatin digestion method. *Journal of reproduction and fertility* **1970**, *23*, 481 –485.

[45] Cerda, J. J.; Brooks, F. P.; Prockop, D. J. Intraduodenal Hydrolysis of Gelatin as a Measure of Protein Digestion in Normal Subjects and in Patients with Malabsorption Syndromes. *Gastroenterology* **1968**, *54*, 358–365.

[46] Correll, J. T.; Vanderpoel, J. C. Biologic Absorption of Insolubilized Gelatin Films. *Proceedings of the Society for Experimental Biology and Medicine* **1949**, *71*, 134 –136.

[47] Huntter, E.; Fell, J.; Sharma, H. The gastric emptying of hard gelatin capsules. *International Journal of Pharmaceutics* **1983**, *17*, 59–64.

[48] Li, Y.; Li, X.; Zhang, Y.; Wang, X.; Wang, Y.; Zhang, Y.; Wang, Y.; Zhang, Y.; Wang, X.; Wang, Y.; Zhang, Y.; Wang, Y. Preparation of Bovine Hides Gelatin by Ultra-High Pressure Technique and the Effect of Its Replacement Fat on the Quality and In Vitro Digestion of Beef Patties. *Foods* **2023**, *12*, 30–92.

[49] Sha, X.-M.; Fang, T.; Zhang, J.-H.; Shu, S.; Jiang, W.-L.; Hu, Z.-Z.; Tu, Z.-C. In vitro gastrointestinal digestion of thermally reversible and irreversible fish gelatin induced by microbial transglutaminase. *Food Hydrocolloids* **2023**, *145*.

[50] Chen, Y.; Wang, Y.; Liu, R.; Xiong, S.; Xu, Y.; Hu, Y. Effects of microbial transglutaminase on the gelling property and in vitro digestibility of fish scale gelatin from grass carp. *Food Bioscience* **2023**, *53*.

[51] Byeon, J. H.; Kang, Y.-R.; Chang, Y. H. Physicochemical and in vitro digestion properties of gelatin/low-methoxyl pectin synbiotic microgels co-encapsulating Lacticaseibacillus casei and pectic oligosaccharides via double-crosslinking with transglutaminase and calcium ions. *Food Hydrocolloids* **2023**, *142*.

[52] Yapo, B. M.; Lerouge, P.; Thibault, J.-F.; Ralet, M.-C. Pectins from citrus peel cell walls contain homogalacturonans homogenous with respect to molar mass, rhamnogalacturonan I and rhamnogalacturonan II. *Carbohydrate Polymers* **2007**, *69*, 426 –435.

[53] Schols, H.; Voragen, A. In *Pectins and Pectinases*, Visser, J, Voragen, A., Eds.; Progress in Biotechnology, Vol. 14; Elsevier: 1996, 3–19.

[54] Levigne, S; Thomas, M; Ralet, M.-C; Quemener, B; Thibault, J.-F Determination of the degrees of methylation and acetylation of pectins using a C18 column and internal standards. *Food Hydrocolloids* **2002**, *16*, 547–550.

[55] Ling Liang, W.; song Liao, J.; Qi, J.-R.; xin Jiang, W.; quan Yang, X. Physicochemical characteristics and functional properties of high methoxyl pectin with different degree of esterification. *Food Chemistry* **2022**, *375*, 131–806.

[56] Thakur, B. R.; Singh, R. K.; Handa, A. K.; and, M. A. R. Chemistry and uses of pectin A review. *Critical Reviews in Food Science and Nutrition* **1997**, *37*, 47–73.

[57] Begum, R.; Aziz, M. G.; Yusof, Y. A.; Saifullah, M.; Uddin, M. B. Evaluation of gelation properties of jackfruit (Artocarpus heterophyllus) waste pectin. *Carbohydrate Polymer Technologies and Applications* **2021**, *2*, 100–160.

[58] Morris, E.; Powell, D.; Gidley, M.; Rees, D. Conformations and interactions of pectins: I. Polymorphism between gel and solid states of calcium polygalacturonate. *Journal of Molecular Biology* **1982**, *155*, 507–516.

[59] Fraeye, I.; Duvetter, T.; Doungla, E.; Van Loey, A.; Hendrickx, M. Fine-tuning the properties of pectin-calcium gels by control of pectin fine structure, gel composition and environmental conditions. *Trends in Food Science & Technology* **2010**, *21*, 219–228.

[60] Luzio, G. A.; Cameron, R. G. Demethylation of a model homogalacturonan with the salt-independent pectin methylesterase from citrus: Part II. Structure-function analysis. *Carbohydrate Polymers* **2008**, *71*, 300–309.

[61] Assifaoui, A.; Lerbret, A.; Uyen, H. T. D.; Neiers, F.; Chambin, O.; Loupiac, C.; Cousin, F. Structural behaviour differences in low methoxy pectin solutions in the presence of divalent cations (Ca2+ and Zn2+): a process driven by the binding mechanism of the cation with the galacturonate unit. *Soft Matter* **2015**, *11*, 551–560.

[62] Grant, G. T.; Morris, E. R.; Rees, D. A.; Smith, P. J.; Thom, D. Biological interactions between polysaccharides and divalent cations: The egg-box model. *FEBS Letters* **1973**, *32*, 195–198.

[63] Tan, J.; McKenzie, C.; Potamitis, M.; Thorburn, A. N.; Mackay, C. R.; Macia, L. In Alt, F. W., Ed.; Advances in Immunology, Vol. 121; Academic Press: 2014, 91–119.

[64] Salyers, A.; Vercellotti, J.; West, S.; Wilkins, T. Fermentation of mucin and plant polysaccharides by strains of Bacteroides from the human colon. *Applied and Environmental Microbiology* **1977**, *33*, 319 –322.

[65] Cao, W.; Guan, S.; Yuan, Y.; Wang, Y.; Mst Nushrat, Y.; Liu, Y.; Tong, Y.; Yu, S.; Hua, X. The digestive behavior of pectin in human gastrointestinal tract: a review on fermentation characteristics and degradation mechanism. *Critical Reviews in Food Science and Nutrition* **2024**, *64*, 12500 –12523.

[66] Mcburney, M.; Horvath, P.; Jeraci, J.; Van Soest, P. Effect of in vitro fermentation using human faecal inoculum on the water-holding capacity of dietary fibre. *British Journal of Nutrition* **1985**, *53*, 17 –24.

[67] Bang, S.-J.; Kim, G.; Lim, M. Y.; Song, E.-J.; Jung, D.-H.; Kum, J.-S.; Nam, Y.-D.; Park, C.-S.; Seo, D.-H. The influence of in vitro pectin fermentation on the human fecal microbiome. *AMB Express* **2018**, *8*.

[68] Li, A.; Shewan, H. M.; Flanagan, B. M.; Williams, B. A.; Mikkelsen, D.; Gidley, M. J. Impact of pectin and alginate gel particle size and concentration on in vitro gut fermentation. *Food Hydrocolloids* **2025**, *160*, 110808.

[69] LeCun, Y.; Bottou, L.; Bengio, Y.; Haffner, P. Gradient-based learning applied to document recognition. *Proceedings of the IEEE* **1998**, *86*, 2278–2324.

[70] Gupta, A. Current Research Opportunities for Image Processing and Computer Vision. *Computer Science* **2019**, *20*, 387–410.

[71] Loutfi, A.; Coradeschi, S.; Mani, G. K.; Shankar, P.; Rayappan, J. B. B. Electronic noses for food quality: A review. *Journal of Food Engineering* **2015**, *144*, 103–111.

[72] Ahlawat, V.; Sharma, R.; Urush Optimizing Gastrointestinal Diagnostics: A CNN-Based Model for VCE Image Classification, 2024.

[73] Hosain, A. S.; Islam, M.; Mehedi, M. H. K.; Kabir, I. E.; Khan, Z. T. In *2022 IEEE 13th Annual Information Technology, Electronics and Mobile Communication Conference (IEMCON)*, IEEE: 2022, 280–285.

[74] Hunter, J. L.; Wicker, L. De-esterification of pectin by alkali, plant and fungal pectinmethylesterases and effect on molecular weight. *Journal of the Science of Food and Agriculture* **2005**, *85*, 2243–2248.

[75] Rosenbohm, C.; Lundt, I.; Christensen, T.; Young, N. Chemically methylated and reduced pectins: preparation, characterisation by 1H NMR spectroscopy, enzymatic degradation, and gelling properties. *Carbohydrate Research* **2003**, *338*, 637–649.

[76] Mao, L.; Ma, L.; Fu, Y.; Chen, H.; Dai, H.; Zhu, H.; Wang, H.; Yu, Y.; Zhang, Y. Transglutaminase modified type A gelatin gel: The influence of intra-molecular and inter-molecular cross-linking on structure-properties. *Food Chemistry* **2022**, *395*, 133–578.

[77] Draget, K. I.; Østgaard, K.; Smidsrød, O. Alginate-based solid media for plant tissue culture. *Applied Microbiology and Biotechnology* **1989**, *31*, 79–83.

[78] Maire du Poset, A.; Zitolo, A.; Cousin, F.; Assifaoui, A.; Lerbret, A. Evidence for an egg-box-like structure in iron(ii)-polygalacturonate hydrogels: a combined EXAFS and molecular dynamics simulation study. *Phys. Chem. Chem. Phys.* **2020**, *22*, 2963–2977.

[79] Chatjigakis, A.; Pappas, C; N.Proxenia; O.Kalantzi; P.Rodis; Polissiou, M FT-IR spectroscopic determination of the degree of esterification of cell wall pectins from stored peaches and correlation to textural changes. *Carbohydrate Polymers* **1998**, *37*, 395–408.

[80] Fellah, A.; Anjukandi, P.; Waterland, M. R.; Williams, M. A. Determining the degree of methylesterification of pectin by ATR/FT-IR: Methodology optimisation and comparison with theoretical calculations. *Carbohydrate Polymers* **2009**, *78*, 847–853.

[81] Renard, C. M.; Crépeau, M.-J.; Thibault, J.-F. Structure of the repeating units in the rhamnogalacturonic backbone of apple, beet and citrus pectins. *Carbohydrate Research* **1995**, *275*, 155–165.

[82] Macleod, G. S.; Collett, J. H.; Fell, J. T. The potential use of mixed films of pectin, chitosan and HPMC for bimodal drug release. *Journal of Controlled Release* **1999**, *58*, 303–310.

[83] Francis, S.; Kumar, M.; Varshney, L. Radiation synthesis of superabsorbent poly(acrylic acid)-carrageenan hydrogels. *Radiation Physics and Chemistry* **2004**, *69*, 481–486.

[84] Nielsen, P.; Petersen, D.; Dambmann, C. Improved Method for Determining Food Protein Degree of Hydrolysis. *Journal of Food Science* **2001**, *66*, 642–646.

[85] Karlsson, J.; Lopez-Sanchez, P.; Marques, T. M.; Hyötyläinen, T.; Castro-Alves, V.; Krona, A.; Ström, A. Effect of heating of pea fibres on their swelling, rheological properties and in vitro colon fermentation. *Food Hydrocolloids* **2024**, *147*, 109–306.

[86] Dei Cas, M.; Paroni, R.; Saccardo, A.; Casagni, E.; Arnoldi, S.; Gambaro, V.; Saresella, M.; Mario, C.; La Rosa, F.; Marventano, I.; Piancone, F.; Roda, G. A straightforward LC-MS/MS analysis to study serum profile of short and medium chain fatty acids. *Journal of Chromatography B: Analytical Technologies in the Biomedical and Life Sciences* **2020**, *1154*, 121982.

[87] Alavarse, A. C.; Frachini, E. C. G.; da Silva, R. L. C. G.; Lima, V. H.; Shavandi, A.; Petri, D. F. S. Crosslinkers for polysaccharides and proteins: Synthesis conditions, mechanisms, and crosslinking efficiency, a review. *International Journal of Biological Macromolecules* **2022**, *202*, 558–596.

[88] Omidian, H.; Park, K. In *Biomedical Applications of Hydrogels Handbook*; Springer New York: New York, NY, 2010; Chapter Introduction to Hydrogels, 1–16.

[89] Wang, L.; Liang, Q.; Chen, Q.; Xu, J.; Shi, Z.; Wang, Z.; Liu, Y.; Ma, H. Hydrolysis kinetics and radical-scavenging activity of gelatin under simulated gastrointestinal digestion. *Food Chemistry* **2014**, *163*, 1–5.

[90] Alemán, A.; Giménez, B.; Gómez-Guillén, M. C.; Montero, P. Enzymatic hydrolysis of fish gelatin under high pressure treatment. *International Journal of Food Science and Technology* **2011**, *46*, 1129–1136.

[91] Ao, J.; Li, B. Amino acid composition and antioxidant activities of hydrolysates and peptide fractions from porcine collagen. *Food Science and Technology International* **2012**, *18*, 425–434.

[92] Nhari, R. M. H. R.; Yaakob, C. M.; Ismail, A.; A., N. Chemical and functional properties of bovine and porcine skin gelatin. *International Food Research Journal* **2011**, *18*, 787–791.

[93] Renard, C. M.; Thibault, J.-F. Degradation of pectins in alkaline conditions: kinetics of demethylation. *Carbohydrate Research* **1996**, *286*, 139–150.

[94] KIRTCHEV, N.; PANCHEV, I.; KRATCHANOV, C. Kinetics of acid-catalysed de-esterification of pectin in a heterogeneous medium. *International Journal of Food Science & Technology* **1989**, *24*, 479–486.

[95] Assifaoui, A.; Lerbret, A.; Uyen, H. T. D.; Neiers, F.; Chambin, O.; Loupiac, C.; Cousin, F. Structural behaviour differences in low methoxy pectin solutions in the presence of divalent cations (Ca2+ and Zn2+): a process driven by the binding mechanism of the cation with the galacturonate unit. *Soft Matter* **2015**, *11*, 551–560.

[96] Zhao, Y.; Bi, J.; Yi, J.; Wu, X.; Ma, Y.; Li, R. Pectin and homogalacturonan with small molecular mass modulate microbial community and generate high SCFAs via in vitro gut fermentation. *Carbohydrate Polymers* **2021**, *269*.

[97] Mao, G.; Li, S.; Orfila, C.; Shen, X.; Zhou, S.; Linhardt, R. J.; Ye, X.; Chen, S. Depolymerized RG-I-enriched pectin from citrus segment membranes modulates gut microbiota, increases SCFA production, and promotes the growth of Bifidobacterium spp., Lactobacillus spp. And Faecalibaculum spp. *Food and Function* **2019**, *10*, 7828 –7843.

[98] Ferreira-Lazarte, A.; Kachrimanidou, V.; Villamiel, M.; Rastall, R. A.; Moreno, F. J. In vitro fermentation properties of pectins and enzymatic-modified pectins obtained from different renewable bioresources. *Carbohydrate Polymers* **2018**, *199*, 482 –491.

[99] Dongowski, G.; Lorenz, A.; Proll, J. The degree of methylation influences the degradation of pectin in the intestinal tract of rats and in vitro. *Journal of Nutrition* **2002**, *132*, 1935 –1944.

[100] Larsen, N.; De Souza, C. B.; Krych, L.; Cahú, T. B.; Wiese, M.; Kot, W.; Hansen, K. M.; Blennow, A.; Venema, K.; Jespersen, L. Potential of pectins to beneficially modulate the gut microbiota depends on their structural properties. *Frontiers in Microbiology* **2019**, *10*.